

## Quantitative Whole-Body Imaging of I-124-Labeled Adeno-Associated Viral Vector Biodistribution in Nonhuman Primates

Douglas J. Ballon,<sup>1,2,†,\*</sup> Jonathan B. Rosenberg,<sup>2,†</sup> Edward K. Fung,<sup>1</sup> Anastasia Nikolopoulou,<sup>1</sup> Paresh Kothari,<sup>1</sup> Bishnu P. De,<sup>2</sup> Bin He,<sup>1</sup> Alvin Chen,<sup>2</sup> Linda A. Heier,<sup>3</sup> Dolan Sondhi,<sup>2</sup> Stephen M. Kaminsky,<sup>2</sup> Paul David Mozley,<sup>1</sup> John W. Babich,<sup>1</sup> and Ronald G. Crystal<sup>2</sup>

<sup>1</sup>Department of Radiology, Citigroup Biomedical Imaging Center; <sup>2</sup>Department of Genetic Medicine; <sup>3</sup>Department of Radiology; Weill Cornell Medical College, New York, New York, USA.

<sup>†</sup>These two authors contributed equally to this work.

A method is presented for quantitative analysis of the biodistribution of adeno-associated virus (AAV) gene transfer vectors following *in vivo* administration. We used iodine-124 (I-124) radiolabeling of the AAV capsid and positron emission tomography combined with compartmental modeling to quantify whole-body and organ-specific biodistribution of AAV capsids from 1 to 72 h following administration. Using intravenous (IV) and intracisternal (IC) routes of administration of AAVrh.10 and AAV9 vectors to nonhuman primates in the absence or presence of anticapsid immunity, we have identified novel insights into initial capsid biodistribution and organ-specific capsid half-life. Neither I-124-labeled AAVrh.10 nor AAV9 administered intravenously was detected at significant levels in the brain relative to the administered vector dose. Approximately 50% of the intravenously administered labeled capsids were dispersed throughout the body, independent of the liver, heart, and spleen. When administered by the IC route, the labeled capsid had a half-life of ~10 h in the cerebral spinal fluid (CSF), suggesting that by this route, the CSF serves as a source with slow diffusion into the brain. For both IV and IC administration, there was significant influence of pre-existing anticapsid immunity on I-124-capsid biodistribution. The methodology facilitates quantitative *in vivo* viral vector dosimetry, which can serve as a technique for evaluation of both on- and off-target organ biodistribution, and potentially accelerate gene therapy development through rapid prototyping of novel vector designs.

**Keywords:** adeno-associated viral vectors, vector biodistribution, vector immune response, vector dosimetry, AAV imaging

### INTRODUCTION

RECOMBINANT ADENO-ASSOCIATED VIRUS (AAV) vectors are small, single-stranded DNA parvoviruses, in which the viral genes are replaced by an expression cassette containing a transgene of therapeutic interest.<sup>1–3</sup> AAV vectors are widely used for *in vivo* gene delivery,<sup>1–6</sup> have minimal pathogenicity, and mediate persistent expression for the life of nonproliferating cells.<sup>1–3,6–12</sup> The target organ(s), capsid structure, route of administration, and preexisting immunity can each modify the biodistribution of the administered therapeutic vector.<sup>3,13–19</sup>

One of the challenges in developing AAV vectors for specific therapies is how to effectively assess the biodistribution of the vector following *in vivo* administration.<sup>20</sup> The standard approach is to assess vector DNA in various

organs in the experimental animal after necropsy or biopsy.<sup>5,6,13,16,21–24</sup> Most AAV biodistribution data are from rodents,<sup>5,6,13,19,24,25</sup> with limited data from nonhuman primates (NHP)<sup>8,17,26–32</sup> and humans.<sup>33</sup>

We have developed a strategy to radioiodinate AAV capsids with iodine-124 (I-124), a cyclotron-produced positron emitter, with a physical half-life of 4.18 days, which allows for positron emission tomography (PET) of vector biodistribution for several days after I-124-labeled AAV vector administration.<sup>34–36</sup> Our previous study in rodents demonstrated the feasibility and safety of this approach.<sup>37</sup>

In the present study, we scaled up the labeling technique and used quantitative PET imaging to assess the initial biodistribution of I-124-labeled AAV capsids in NHP, a species large enough to facilitate assessment of

\*Correspondence: Dr. Douglas J. Ballon, Departments of Radiology and Genetic Medicine, Weill Cornell Medical College, 1300 York Avenue, Box 164, New York, NY 10065, USA. E-mail: geneticmedicine@med.cornell.edu

vector biodistribution to specific organs. After adjustment for physical half-life, measurements of positron-electron annihilation photons from I-124 decay are a surrogate for the amount of vector capsid present and can be used to calculate whole-body and organ biodistribution as well as the time dependence of capsid metabolism over several days.<sup>38</sup> Capsid metabolism here is defined as the biological half-life of the protein capsid.

As examples, we assessed the biodistribution of I-124-labeled AAVrh.10 and AAV9 vectors administered by either intravenous (IV) or intracisternal (IC) routes to NHP using an observation period of 1–72 h in the absence or presence of systemic anticapsid immunity. We describe our observations in the context of a simple compartmental model that treats multiple organ distribution from a single-source component. The analysis provides new insights into the biodistribution of the two AAV serotypes via the two routes of delivery, observations that should be useful in translating AAV vector use to treat human disease.

## METHODS

### AAV vectors

Four AAV vectors were used: (1) AAVrh.10mCherry, rh.10 capsid, coding for an artificial marker protein, mCherry<sup>39</sup>; (2) AAVrh.10FXN, rh.10 capsid, coding for human frataxin (FXN), a nonsecreted mitochondrial protein; (3) AAV9 mCherry, 9 capsid, coding for mCherry; and (4) AAV9FXN, 9 capsid, coding for human FXN. The two different reporter transgenes were used to avoid inducing antitransgene immunity with a second administration. Each AAV vector contained an expression cassette comprising the cytomegalovirus/ $\beta$ -actin hybrid (CAG) promoter, the transgene cDNA, and the rabbit  $\beta$ -globin poly (A) sequence flanked by AAV2 inverted terminal repeats and encapsidation signal, pseudotyped with either the AAVrh.10 or AAV9 capsid of choice (Supplementary Fig. S1).

HEK 293T cells were cotransfected with the transgene expression cassette plasmid and the packaging/helper plasmid that expresses *in trans* the AAV serotype-specific cap and rep genes, together with the adenovirus helper genes necessary for virus replication and production.<sup>12,40–44</sup> Viral particles were purified using standard methods and concentrated to  $10^{13}$  gene copies per milliliter in phosphate-buffered saline (PBS).<sup>12,43</sup> The production of AAV vectors met the endotoxin, mycoplasma, sterility, and transgene expression release criteria.

### Radioiodination

The use of iodine was based on its relatively mild chemistry for coupling to proteins. We chose the isotope I-124 for its 4-day half-life to allow the measure of vector distribution for several days after administration. NaI-124 was received as a 0.05 M NaOH solution (3D Imaging, Little Rock, AR). Radioiodine solution was neutralized

using pH 7.5, 25 mM Tris HCl buffer containing 0.4 M NaCl and transferred to a Pierce™ Iodogen tube (Thermo Fisher Scientific, Waltham, MA) and kept for 30 min at 23°C with intermittent stirring. The activated NaI-124 solution was transferred to a separate vial containing the AAV9 or AAVrh.10 vector. After mixing, the vial was kept on an ice bath and mixed periodically by gently stirring over 90 min. Following radiolabeling, the product mixture was diluted in pH 9.0, 50 mM Tris HCl, 50 mM NaCl, and purified using an anion exchange cartridge (1 mL, HiTrap Q High Performance cartridge; GE Healthcare, Chicago, IL) followed by centrifugal filtration on 100K MW cutoff filters (Millipore, St Louis, MO) and serial washings (four times) with pH 7.4 PBS buffer at 3,300 rpm for 3 min.

The purified I-124-labeled AAV vectors were formulated in PBS buffer. The labeling efficiency (before purification) and radiochemical purity (after purification) were determined by instant thin-layer chromatography using glass-fiber silica gel paper strips (Agilent Technologies, Santa Clara, CA) as stationary and PBS as mobile phase. The radiolabeling yields (the fraction of the original amount of vector that was in the final product) ranged from 25% to 35%. Purification resulted in >99% radiochemically pure I-124-AAV in all cases that were released for administration, indicating that the amount of free I-124 in the preparation was <1%. Sodium dodecyl sulfate–polyacrylamide gel electrophoresis (SDS-PAGE) demonstrated that 95% of labeled protein included all three (VP1–3) of the AAV capsid proteins (not shown).

An example of the calculation of the number of I-124 atoms per AAV capsid is as follows. Starting with 5.0 mCi of I-124 and  $1.0 \times 10^{13}$  virus particles, the radiochemical labeling procedure was carried out using the Iodogen method as described above.<sup>45</sup> In the final product, 550  $\mu$ Ci was observed in solution with  $3.7 \times 10^{12}$  virus particles. The total number of radioactive atoms in the product was calculated as  $A_0\tau$  where  $A_0 = 550 \mu$ Ci and  $\tau$  is the lifetime that is related to the I-124 half-life by  $\tau = T_{1/2}/0.693$ . Since the radiochemical purity of the product was >99%, the total number of radioactive atoms bound to the AAV capsids was  $7.95 \times 10^{12}$ , and the mean number of I-124 atoms per virus particle in the preparation was 2.15. An overview of the experimental design and the details of the vector labeling for each administration are provided in Table 1.

### Nonhuman primates

The study was carried out with adult male *Chlorocebus aethiops sabaeus* NHP (African green monkeys, [ $n = 6$ ]; 5- to 7-year old; 5.5–8.5 kg; Worldwide Primates, Miami, FL). All monkeys were healthy and pathogen free during the 3-month quarantine and subsequent study periods. No animal had been previously used for experimental studies. NHP were maintained in paired-housed cages, fed twice daily with monkey chow (Monkey Diet Jumbo; PMI Nutrition International, Brentwood, MO), supplemented

**Table 1.** I-124-AAVrh.10 and 9 vector positron emission tomography imaging in nonhuman primates

NHP No. <sup>a</sup>	Route	Vector Immune Status <sup>b</sup>	AAV Serotype/Transgene <sup>c</sup>	Day of Vector Administration	Labeled Activity, $\mu\text{Ci}$	Injected Activity, $\mu\text{Ci}$	Dose of Vector Administered, gc	Ratio of AAV dose to Injected Activity, gc/ $\mu\text{Ci}$	I-124 per Capsid	Detected Activity, $\mu\text{Ci}$ <sup>d</sup>
1	Intravenous	Naive	10/mCherry	0	243	150	$3.1 \times 10^{12}$	$2.1 \times 10^{10}$	1.51	99
		Immune	10/FXN	63	1060	748	$6.6 \times 10^{12}$	$0.9 \times 10^{10}$	3.10	520
2	Intravenous	Naive	9/mCherry	0	110	59	$5.7 \times 10^{12}$	$9.7 \times 10^{10}$	0.37	40
		Immune	9/FXN	70	656	350	$4.2 \times 10^{12}$	$1.2 \times 10^{10}$	3.01	292
3	Intracisternal	Naive	10/mCherry	0	727	437	$5.0 \times 10^{12e}$	$1.1 \times 10^{10e}$	2.80 <sup>e</sup>	351
		Immune	10/FXN	70	950	689	$5.0 \times 10^{12}$	$0.7 \times 10^{10}$	3.66	542
4	Intracisternal	Naive	9/mCherry	0	550	413	$3.7 \times 10^{12}$	$0.9 \times 10^{10}$	2.87	325
		Immune	9/FXN	91	420	278	$1.1 \times 10^{13}$	$4.0 \times 10^{10}$	0.74	258
5	Intracisternal	Naive	9/mCherry <sup>f</sup>	0	624	500	$5.5 \times 10^{13}$	$1.1 \times 10^{11}$	2.41	397
6	Intracisternal	Nal control	I-124-Nal	0	NA	410	—	—	—	281
	Intravenous	Nal control	I-124-Nal	112	NA	26	—	—	—	419

The initial I-124 calibrated activity for each experiment was 5.0 mCi, and the initial viral titer was  $\sim 1 \times 10^{13}$  gc. PET/CT was performed 1, 24, 48, and 72 h after I-124-labeled vector administration.

<sup>a</sup>All NHP (African green monkeys), adult males (5–7 years; 5.5–8.5 kg); total of  $n=6$  NHP were administered with  $n=1$ /serotype/route plus  $n=1$  control for free I-124 activity. For NHP1–4, each was administered an I-124-labeled vector twice, with the second administration 63 to 91 days later; for NHP6 (Nal control), I-124-Nal was administered twice (different routes), with the second administered at 112 days.

<sup>b</sup>NHP immunity status. For the initial vector administration, the NHP were immune-naive to the capsid; at the time of the second administration with the same capsid, the NHP had developed immunity against the capsid (Figs. 3A, B and 9A, B); the Nal control remained capsid immune-naive.

<sup>c</sup>Vectors tested were AAV9 (9) or AAVrh.10 (10) serotypes, with mCherry transgene for initial exposure, and human FXN transgene for the second immunized round of imaging.

<sup>d</sup>Activity measured from the 1-h PET scan on day 0.

<sup>e</sup>Viral titer not performed for NHP3; the titer is an estimated value based upon the use of the same initial vector titer that was used for the other labeling experiments and resulting image quality.

<sup>f</sup>NHP5 received a total vector dose  $\sim 10 \times$  higher ( $5.5 \times 10^{13}$  gc, compared with  $\sim 5 \times 10^{12}$  gc for NHP1–4). mCherry protein was assessed in this NHP at 6 weeks.

AAV, adeno-associated virus; CT, computed tomography; FXN, frataxin; I-124, iodine-124; NHP, nonhuman primates; PET, positron emission tomography.

with fruit or vegetables daily, with access to water *ad libitum*, enriched with videos, toys, and observed daily by the research specialists for general appearance, signs of toxicity, distress, and changes in behavior. All studies were conducted under protocols reviewed and approved by the Weill Cornell Institutional Animal Care and Use Committee (Protocol No. 2013-0022) following NIH guide for care and use of laboratory animals, including the use of I-124. We chose African green monkeys due to their similarity to human physiology and scalability to humans, and our extensive behavioral and blood parameter data sets from our prior NHP AAV studies.<sup>11,12,43,46,47</sup>

### Study design

The design of this study included AAV serotypes previously investigated in multiple NHP studies to address the initial distribution of the AAV in the whole body.<sup>11,12,26,30–32,43,46,48–52</sup> We chose a moderate AAV dose (average total dose  $4.4 \times 10^{12}$  I-124-labeled AAV vector capsids) for the initial trial design that allowed good visualization of the PET signal of I-124 radiolabeled AAV, and to limit the amount of radioactivity injected into the animals. All NHP were screened for seropositivity against AAV9 and AAVrh.10 before inclusion in the study to insure that no NHP exhibited total or neutralizing anti-AAV antibodies. The capsid serotype, transgene, route of vector administration, and immune status for each NHP were as follows. NHP1, AAVrh.10mCherry, IV administration, capsid immune-

naive, followed in 63 days with AAVrh.10FXN, IV, capsid immune. NHP2, AAV9mCherry, IV, capsid immune-naive, followed in 70 days with AAV9FXN, IV, capsid immune. NHP3, AAVrh.10mCherry, IC, capsid immune-naive, followed in 70 days with AAVrh.10FXN, IC, capsid immune. NHP4, AAV9mCherry, IC, capsid immune-naive, followed in 91 days with AAV9FXN, IC, capsid immune. NHP5, AAV9mCherry, IC, capsid immune-naive, higher dose, used for additional assessment at 42 days for organ levels of mCherry. NHP6, I-124-Nal control, IC, capsid immune-naive, followed in 112 days with I-124-Nal control, IV, capsid immune-naive. All AAV vectors (AAV9, AAVrh.10) or PBS sham was administered via aseptic procedures.

Following administration of the I-124 infusate to the NHP, the animals were monitored for adverse reactions  $3 \times$ /day for the first week and then daily afterward. No animal displayed adverse events. Radioactivity was monitored in the cage and wastes daily. After 72 h, no activity was detected in the excreted waste.

### Vector administration

**IV administration.** Anesthetized NHP were placed in supine position, the saphenous vein shaved and scrubbed for IV injection, and a sterile drape placed over the animal with the site exposed. A SurgiVet (22G 1") vascular catheter (Waukesha, WI) was placed in the right or left lateral saphenous vein. The catheter was then secured in place with tape and patency verified by injecting a

heparin flush solution. The NHP was transported to the PET/CT (computed tomography) imaging room at the Citigroup Biomedical Imaging Center and placed in a right-side lateral recumbency position on a raised platform atop the scan bed, perpendicular to the scanner bore axis to allow for whole-body PET imaging. Immediately before the initiation of the scan, the injectate (1.0 mL) was slowly administered via catheter port (0.5 mL/min), followed by 1 mL of saline flush. Leftover vector in the syringe/needle was measured for radioactivity; this amount was subtracted from the original syringe amount to determine the injected activity.

**IC administration.** With the NHP anesthetized, the dorsal upper neck/lower skull area was shaved, the skin scrubbed, and prepped for IC injection. The NHP was transported to the PET/CT imaging room (CBIC) and a sterile drape placed over the animal. While in a lateral decubitus position, the head was held with one hand so that the weight was taken off the spine and the head bent forward. Occiput projections were found by palpation. A spinal needle (22G, 1.5"; Becton Dickinson, Franklin Lakes, NJ) was used to pierce the neck skin medially to the protuberantia occipitalis externa. The needle was then gently guided steeply upward through the neck muscles to the membrane atlanto-occipitalis posterior. The tip of the needle was then inserted into this small gap to pierce the cisterna magna.

The position of needle was confirmed by free flow of clear cerebrospinal fluid back into the needle hub, and by CT imaging of the needle in the cisterna magna before injection of the radiolabeled AAV. For injections, the radioactive infusate syringe was connected to a three-way stop-cock (DiscoFix; B. Braun Medical, Bethlehem, PA) and a T-connector set (6.5" tubing; B. Braun Medical) to allow both the vector and flush to be attached in line to the IC port and spinal needle. Air bubbles were removed from the vector prep and flushed to the tip of the syringe, which was sterilely attached via luer lock to the first port on three-way stop-cock, with the saline flush attached to the second port.

Following cerebral spinal fluid (CSF) collection, the syringe/stop-cock assembly was attached to the spinal needle hub gently as not to move the needle. The injectate (1.0 mL) was slowly administered via catheter port (0.5 mL/min), followed by 1 mL of saline flush as above. Following administration, the needle was slowly removed and gentle pressure was placed over the site. The cisterna magna puncture was self-sealing. Leftover vector in syringe/needle was measured for radioactivity and this amount was subtracted from the initial syringe amount to obtain the injected activity. Afterward, the NHP was placed back into the right-side lateral recumbency position on a raised platform on the scan bed, perpendicular to the scanner bore axis to allow for the entire body to be within

the field-of-view of the PET detectors. The initiation of the PET imaging session began after the CT alignments, ~15–20 min post-I-124/vector infusate injections.

### **Anti-AAV vector total and neutralizing antibody titers**

Serum was collected before AAV administration and then at 2-week intervals afterward. Serum total anti-AAV antibody titers were assessed in AAV9- or AAVrh.10-coated enzyme-linked immunosorbent assay plates, as described previously.<sup>12,40,43</sup> Serum neutralizing anti-AAV antibody titers were assessed in 293ORF6 cells by measuring inhibition of AAV9- or AAVrh.10-mediated luciferase transgene expression.<sup>11,12,40,43</sup>

### **Positron emission tomography**

All images were acquired using a Siemens Biograph mCT PET/CT Scanner system (Siemens, Erlangen, Germany) equipped with four PET detector rings. For each imaging session, 1 h of dynamic PET imaging was performed in list-mode immediately following CT scans. List-mode raw data were reframed and reconstructed with CT-based attenuation, scatter, and a point-spread-function with time-of-flight compensations. Each NHP underwent PET imaging scans on four successive days under general anesthesia, at 1, 24, 48, and 72 h after vector administration. For the IV administrations, the animals were injected while already positioned in the PET scanner, with imaging started immediately. For the IC administrations, additional procedural maneuvering was required once the spinal needle was removed and animal intubated, and the imaging was started ~20 min following I-124-AAV vector infusions.

The PET scanner was calibrated in Bq/mL on a quarterly basis, using a source of known activity comprising deoxyglucose fluorinated with the positron emitter fluorine-18 in solution. The calibrated activity was injected into a phantom approved by the American College of Radiology. All measurements in Bq/mL on the scanner were within 1% of the calibrated source value over the time period of the NHP experiments, which was ~9 months.

### **Image analysis**

Total activity in each measured organ at each time point was determined by defining volumetric regions-of-interest manually on registered day 0 PET/CT images using the Siemens Inveon Research Workplace software (version 4.2). At a nominal in-plane voxel size of  $2 \times 2 \text{ mm}^2$  and a slice thickness of 5 mm, the activity was summed over the slices containing each organ. The effective spatial resolution for PET radioisotopes is affected by the positron range and detector geometries. For example, a line source of I-124 yields a spatial resolution defined by the full-width-at-half-maximum image intensity of ~5–6 mm for human PET scanner detector configurations.<sup>53–56</sup> Later

time point images were registered with day 0 images using a manual rigid transformation. For whole-body measurements, an effective half-life of I-124 ( $T_{1/2 \text{ eff}}$ ) was calculated by fitting a monoexponential function to the longitudinal data. Biological half-lives were calculated from the effective half-lives as  $1/T_{1/2 \text{ bio}} = 1/T_{1/2 \text{ eff}} - 1/T_{1/2 \text{ phys}}$ , where  $T_{1/2 \text{ phys}}$  is the physical half-life of I-124 (100.32 h).

### Vector dosimetry

A simple compartmental model was applied to time-activity curves for each NHP to facilitate the determination of organ biodistribution. The model assumed a single-source component, which was taken as the blood pool for IV injections and the CSF for IC injections, six-organ compartments, including the liver, heart, vertebrae/bone marrow, spleen, CSF/brain, and a remainder compartment (“body remainder”) that was distributed throughout the body, and two sink compartments, including accumulation in the thyroid and the amount excreted. After correction for physical decay, the time-dependent distribution of I-124 radioactivity after administration was modeled as follows:

$$\begin{aligned} dC_s(t)/dt &= -k_s C_s(t) \\ dC_{oi}(t)/dt &= a_{oi} k_s C_s(t) - k_{oi} C_{oi}(t) \quad (1) \\ dC_{ej}(t)/dt &= a_{ej} (\sum k_{oi} C_{oi}(t)) \end{aligned}$$

where  $C_s(t)$  is the amount of I-124 in the source compartment at time  $t$ , which decays via the biological rate constant  $k_s$ ,  $C_{oi}(t)$  is the amount of I-124 in the  $i$ th organ ( $i=1-6$ ) fed by the source compartment with a distribution fraction  $a_{oi}$  and with decay constant  $k_{oi}$ ,  $C_{ej}(t)$  is the amount of I-124 in the  $j$ th sink compartment ( $j=1-2$ ) fed from the organs with a distribution fraction determined by  $a_{ej}$ . The constraints  $\sum a_{oi} = 1$  and  $\sum a_{ej} = 1$  were applied to the model to enforce conservation of the total number of I-124 atoms at all time points. With these considerations, there are 9 Equations (1) with 13 free model parameters (6 independent distribution fractions and 7 decay constants).

Equations (1) were solved numerically for  $C_s(t)$ ,  $C_{oi}(t)$ , and  $C_{ej}(t)$  using regression by first minimizing the sum of squares of the logarithmic residuals for the organ components over all data points for each I-124 AAV administration, thereby determining the best estimates of  $a_{oi}$  and  $k_{oi}$ . The sink distribution fractions were obtained in a second step, fitting the last two of Equations (1) to the thyroid and excreted component, again minimizing the sum of squares of the logarithmic residuals. The thyroid component was measured directly from a region-of-interest placed over the gland, and the excreted component followed from the conservation of activity relation above.

Biological half-lives of I-124 in organs were calculated from all decay constants  $k$  as  $T_{1/2 \text{ bio}} = 0.693/k$ . In a few cases (AAV9 IV naive, AAVrh.10 IC immune, AAV9 IC naive, AAV9 IC immune), a relaxation of strict enforcement of the time conservation of I-124 activity in the model achieved significantly better fitting to certain organs. This resulted in more accurate calculations of the organ decay half-lives. The violation of time conservation results if all activity is not captured in the region-of-interest selected for each organ at a given time point.

Note that the compartmental model does not distinguish between I-124 bound to capsids, capsid fragments, or unbound I-124.

In addition to the numerical solutions, the nine Equations (1) were solved analytically using matrix formalism that leads to a standard eigenvalue problem. Since Equations (1) are a system of first-order linear-coupled differential equations with constant coefficients, the analytical solutions are straightforward,<sup>57</sup> with all the decay constants appearing as eigenvalues and the distribution fractions as components of the eigenvectors. Analytical and numerical results were compared as a check for consistency by substituting the distribution fractions and decay constants obtained numerically into the functional forms obtained analytically, and then noting any differences between each of the nine numerical and analytical solutions.

In Equation (1) above, the set of coefficients  $a_{oi}$  represents the fractional distribution of administered vector reaching each organ. It is also possible to obtain a simple estimate of the absolute amount of vector delivered to each organ ( $N_{oi}$ ) by

$$N_{oi} = N_v a_{oi} \quad (2)$$

where  $N_v$  is the total amount of vector actually administered. In our case,  $N_v = N_0(A_f/A_0)$  where  $N_0$  is the injected amount of vector including any amount still present in the syringe and catheter after injection, and  $A_f/A_0$  is the ratio of the I-124 activity found in the PET image on day 0 immediately after injection to the I-124 activity measured just before the time of injection in a dose calibrator. Combining both equations yields

$$N_{oi} = N_0(A_f/A_0)a_{oi}. \quad (3)$$

Therefore, for each administration, an estimate of the amount of vector reaching a given organ contains three measured quantities,  $N_0$ ,  $A_f$ , and  $A_0$ , and one model parameter  $a_{oi}$ .

### Statistical considerations

In this study, there was only one NHP per experiment, and thus, a statistical assessment across individuals was not possible. The results pertaining to compartmental

model parameters in individual NHP should therefore be considered preliminary assessments. Measurements of signal-to-noise ratios of I-124 activity for all NHP in all compartments (source, organs, and sink) were based upon nuclear counting (Poisson) statistics. Calculations of chi-square per degree-of-freedom were used to determine the goodness-of-fit of the compartmental model to I-124 activity versus time in organs.

## RESULTS

### IV administration to NHP with no preexisting immunity

Control I-124-NaI administration resulted in distribution primarily to the thyroid, submandibular glands, and parotid glands (Fig. 1A and Table 2). By 48 h, I-124 was mostly in the thyroid and small intestines. The whole-body biological half-life ( $T_{1/2}$ ) of I-124 NaI was 15.6 h, with rapid elimination from all organs and rapid accumulation in the thyroid (Table 3 and Fig. 2A, E).

In marked contrast, after IV administration of both I-124-AAVrh.10 and I-124-AAV9, I-124 activity was distributed primarily to the liver and heart (Figs. 1B, C, and 2B, C; for a 24-h pseudo-three-dimensional view, see Supplementary Video S1). Interestingly, however, there was also distribution to the nose, parotid glands, submandibular glands, spleen, long bones, and vertebrae (Fig. 1B, C). The tropism of both AAVrh.10 and AAV9 for the vertebrae (see Supplementary Fig. S2 for a close-up view) is consistent with reports of AAV distribution to bone and/or bone marrow.<sup>26,27</sup> In addition, despite the success of AAV9-administered IV in treating central nervous system (CNS) disease in infants,<sup>58</sup> in our assessment of adult NHP, <1% of I-124 activity was distributed to the brain for either serotype-administered IV. At 1 h, both vectors were observed in the large vasculature. By 24 h, the thyroid was positive, likely reflecting removal of I-124 from some of the vector capsids.

In general, quantitative analysis of IV administration of I-124-AAVrh.10 and I-124-AAV9 to capsid immune-naive NHP demonstrated that the two vectors behaved in a similar manner with some minor differences. The total body clearance of I-124 was similar, 61.9 h for AAVrh.10 and 54.1 h for AAV9, likely representing a combination of deiodination of the capsid, capsid fragmentation, and urine/bowel elimination (Fig. 2A). The organ fractional distribution was similar, with the liver dominating (18% for rh.10, 41% for 9), with detectable but lower values in the heart, vertebrae, and spleen, and <1% distribution to CSF or brain parenchyma. Interestingly, a significant amount of activity was spread diffusely throughout the body, likely in muscle (65% for rh.10, 45% for 9).

In our analysis, the body fraction specifically represents the I-124 signal detected in sites other than the liver, heart, vertebrae, spleen, and CSF/brain (although visually little

activity was identified in the brain parenchyma, the quantification, dominated >99% by CSF, includes both). I-124 biological half-lives in organs ranged from 15 to 75 h, presumably reflecting the time evolution of capsid metabolism. The skeletal muscle is a known site for distribution of both vectors, but at levels significantly lower per unit mass than the liver.<sup>59,60</sup> In that regard, the quadriceps show distribution of both I-124-AAVrh.10 and I-124-AAV9 to skeletal muscle at a level per unit volume that is considerably lower than the liver (Fig. 1 and Supplementary Fig. S3). In the context that skeletal muscle represents about 40% of the total body mass of primates,<sup>61</sup> this suggests that approximately half of the IV-administered vector is distributed to organs other than the liver, heart, CSF/brain, and spleen, with skeletal muscle representing a significant proportion of the “body remainder.” However, we cannot delineate muscle cells from the extensive microvasculature within the muscle.

Assessment of the fate of I-124-AAVrh.10 and I-124-AAV9 vectors in specific organs following IV administration supported the observation that, in general, the two vectors behaved in a similar manner with some differences (Fig. 2C–E). The biological half-life of the labeled capsid within each organ likely represents capsid metabolism in the form of destruction of the capsid and/or deiodination of the label within the organ. Organ biological half-lives ranged from about 15 to about 70 h, the measurement upper limit of the method. With the caveat that the data are from a single NHP for each serotype, there were differences in the behavior of the two vectors. For example, the liver  $T_{1/2}$  for I-124-AAVrh.10 was 71.2 h versus 22.6 h for I-124-AAV9, while the heart  $T_{1/2}$  was similar for both (rh.10 vs. 9, 15.0 h vs. 15.6 h; Table 3).

### IV administration to NHP with preexisting anticapsid immunity

Systemic immunity against the AAVrh.10 and AAV9 capsids was induced by the first IV administration of the rh.10 and 9 vectors, respectively (Fig. 3A, total anticapsid antibodies; Fig. 3B, neutralizing anticapsid antibodies). Thus, when AAVrh.10FXN was administered IV to NHP1 or AAV9FXN was administered IV to NHP2, the vectors were administered to NHP with preexisting immunity against the relevant capsid. Qualitative analysis of whole-body PET images dramatically demonstrated the consequences of administering an AAV vector IV in the context of significant preexisting immunity versus immune naive status. For example, when compared with administration in nonimmune NHP, there is a marked increase in distribution to the spleen (AAVrh.10FXN; compare Fig. 3C with Fig. 1B).

A similar pattern was seen for AAV9FXN administered to an AAV9 capsid immune NHP (compare Fig. 3D with Fig. 1C). In the immune NHP, the I-124 signal in the bladder is also observed, likely representing free I-124 and/or I-124 fragment clearance.

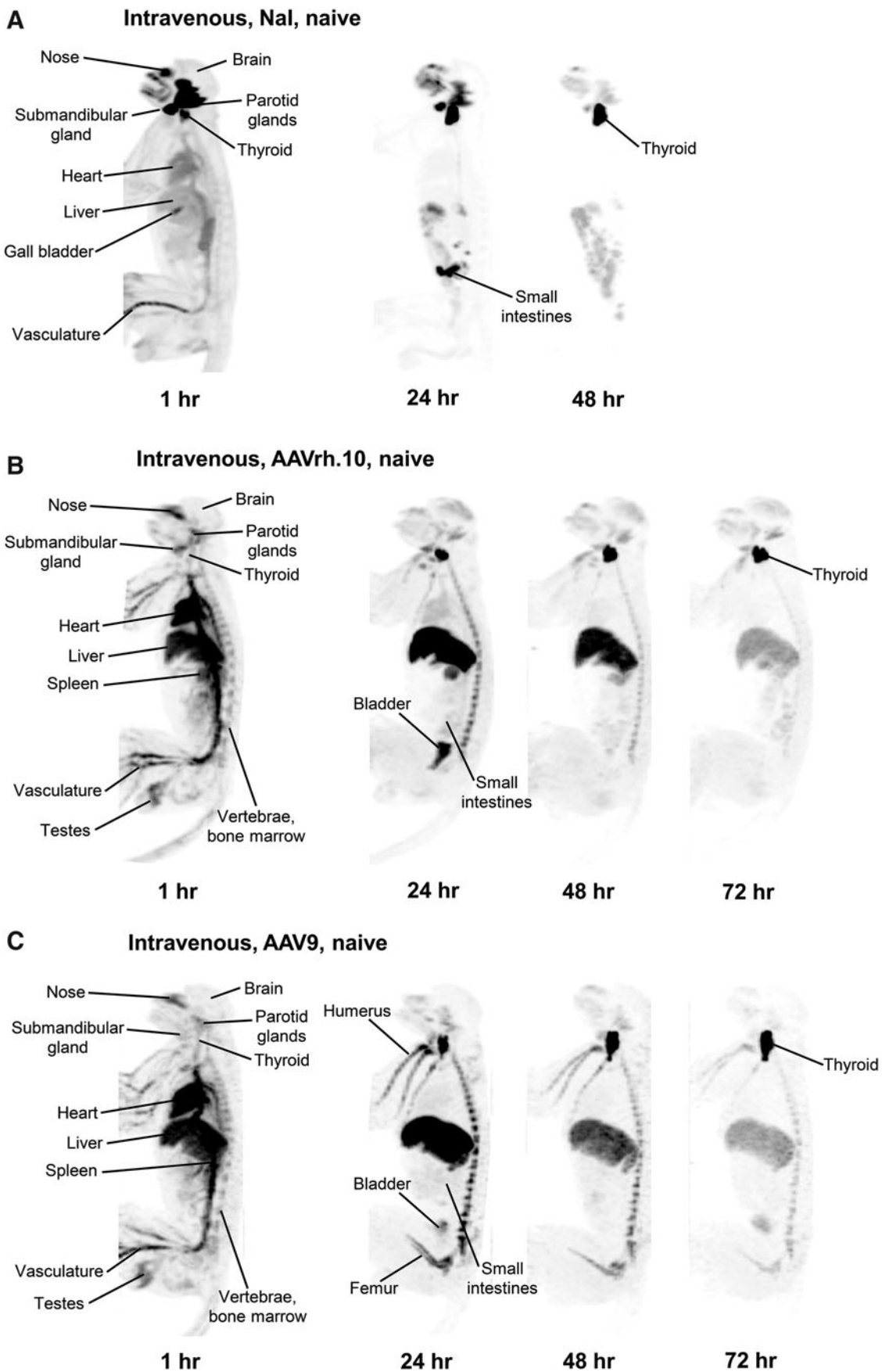


**Figure 1.** PET images of I-124-labeled AAVrh.10 and AAV9 vectors following intravenous administration. For (A–C), the first image is the 1-h image with identification of positive organs; this is followed by images acquired at 24, 48, and 72 h. See Table 1 for details of the dosing of each NHP. (A) Control— intravenous administration of I-124-labeled Nal alone to NHP (NHP6) with no preexisting systemic anticapsid immunity (“naive”). (B) Intravenous administration of I-124-labeled AAVrh.10mCherry, vector immune naive-NHP1. (C) Intravenous administration of I-124-labeled AAV9mCherry, vector immune-naive NHP2. All images are maximum intensity projections normalized to injected activity and corrected for physical decay. AAV, adeno-associated virus; I-124, iodine-124; NHP, nonhuman primates; PET, positron emission tomography.

**Table 2.** I-124 percentage organ biodistribution following administration of I-124-labeled vectors

NHP No. <sup>a</sup>	Route	Vector Immune Status <sup>a</sup>	AAV Serotype/Transgene <sup>a</sup>	Liver	Heart	Vertebrae	Spleen	CSF/Brain	Body <sup>b</sup>
1	Intravenous	Naive	10/mCherry	18.4	11.2	4.2	1.3	0.3	64.6
		Immune	10/FXN	31.5	3.1	5.8	6.1	0.2	53.2
2	Intravenous	Naive	9/mCherry	41.3	5.2	6.3	1.9	0.1	45.1
		Immune	9/FXN	45.4	3.3	4.1	8.6	0.1	38.4
3	Intracisternal	Naive	10/mCherry	12.0	5.0	1.0	0.5	14.0	67.6
		Immune	10/FXN	11.4	2.1	1.8	7.2	14.5	63.0
4	Intracisternal	Naive	9/mCherry	9.4	9.5	0.2	0.5	12.6	67.8
		Immune	9/FXN	26.6	3.2	2.1	6.4	21.5	40.2
5	Intracisternal	Naive	9/mCherry	20.2	5.0	2.6	1.8	4.0	66.4
6	Intracisternal	NaI control	I-124 alone	2.4	1.5	0.4	0.1	0.1	95.4
	Intravenous	NaI control	I-124 alone	6.3	4.5	0.6	0.5	0.1	87.9

The percentage distribution for each organ is equal to  $100 \times a_{oi}$  where the distribution fractions  $a_{oi}$  were calculated from Equation (1).

<sup>a</sup>See Table 1 for description of NHP, immune status, and description of the AAV vectors.

<sup>b</sup>Body activity represents all I-124 activity that was not assigned to the five organs listed or the thyroid. CSF, cerebral spinal fluid.

Quantitative analysis of the distribution of I-124-AAVrh.10 and I-124-AAV9 when administered in the context of systemic capsid immunity demonstrated significant differences compared with administration to a capsid immune-naive recipient. The total body clearance of the I-124 signal was markedly shortened, from 61.9 to 25.6 h for AAVrh.10 and 54.1 to 24.2 h for AAV9 (Fig. 4A). Interestingly, the fractional distribution of the vectors in the context of anticapsid immunity demonstrated increased distribution of both AAVrh.10 and AAV9 to the liver (AAVrh.10 naive 18%, immune 31%; AAV9 naive 41%, immune 45%; Fig. 4B). However, the I-124 was removed more quickly from the liver ( $T_{1/2}$  AAVrh.10 naive 71.2 h, immune 13.1 h; AAV9 naive 22.6 h, immune 10.1 h; Table 3). While a similar shorter half-life was observed in immune animals with AAVrh.10 and AAV9 in the heart and vertebrae, the opposite was seen in the spleen (AAVrh.10 naive 20.6 h, immune 63.0 h; AAV9 naive 22.9 h, immune 83.5 h; Table 3).

### IC administration to NHP with no preexisting anticapsid immunity

As a control, IC administration of I-124-NaI demonstrated distribution to the CSF, nose, parotid glands, and thyroid, with some diffusion to the liver, heart, and bladder. The distribution to the brain was <1%. By 24 to 48 h, most of the I-124-NaI was eliminated, with continued presence, as expected, in the thyroid. In contrast, in NHP with no preexisting immunity (NHP3 for AAVrh.10, NHP4 for AAV9; see Table 1), IC administration of both I-124-AAVrh.10 and I-124-AAV9 demonstrated very different biodistribution compared with the control I-124 NaI and to IV administration of the vectors (Fig. 5). With some quantitative differences, IC administration of I-124-labeled AAVrh.10 and AAV9 capsids was similar (Fig. 5B, C; for a 24-h pseudo-three-dimensional view, see Supplementary Video S2). Both demonstrated distribution to the CSF, primarily the cisterna magna and spinal canal. With the caveat that we only assessed  $n = 1$  per vector, there appears to be increased breadth of the

**Table 3.** I-124 biological half-life of I-124-labeled AAVrh.10 and 9 capsids in selected organs following vector administration

NHP No. <sup>a</sup>	Route	Vector Immune Status <sup>a</sup>	AAV Serotype/Transgene <sup>a</sup>	Biological Half-Life, h						
				Source <sup>b</sup>	Liver	Heart	Vertebrae	Spleen	CSF/Brain	Body
1	Intravenous	Naive	10/mCherry	0.7	71.2	15.0	53.3	20.6	25.7	60.1
		Immune	10/FXN	0.7	13.1	10.8	19.1	63.0	15.9	24.0
2	Intravenous	Naive	9/mCherry	1.2	22.6	15.6	34.0	22.9	24.8	48.7
		Immune	9/FXN	0.8	10.1	9.7	13.2	83.5	13.2	22.8
3	Intracisternal	Naive	10/mCherry	13.9	34.7	11.0	34.7	49.5	12.4	43.3
		Immune	10/FXN	10.7	22.4	12.9	10.9	15.7	7.7	24.6
4	Intracisternal	Naive	9/mCherry	12.8	66.5	12.6	42.3	55.3	26.7	23.1
		Immune	9/FXN	9.6	5.4	5.9	6.1	25.5	7.7	14.1
5	Intracisternal	Naive	9/mCherry	12.5	48.9	23.1	46.2	24.0	4.3	62.8
6	Intracisternal	NaI control	I-124 alone	5.0	14.3	11.3	11.3	13.3	9.9	24.5
	Intravenous	NaI control	I-124 alone	0.7	12.8	9.3	18.0	8.9	14.7	14.5

The biological half-lives (in h) were calculated from decay constants as  $T_{1/2} \text{ bio} = 0.693/k$ .

<sup>a</sup>See Table 1 for description of NHP, immune status, and description of the AAV vectors.

<sup>b</sup>Source of I-124 activity is blood for the intravenous route and CSF for the intracisternal route.

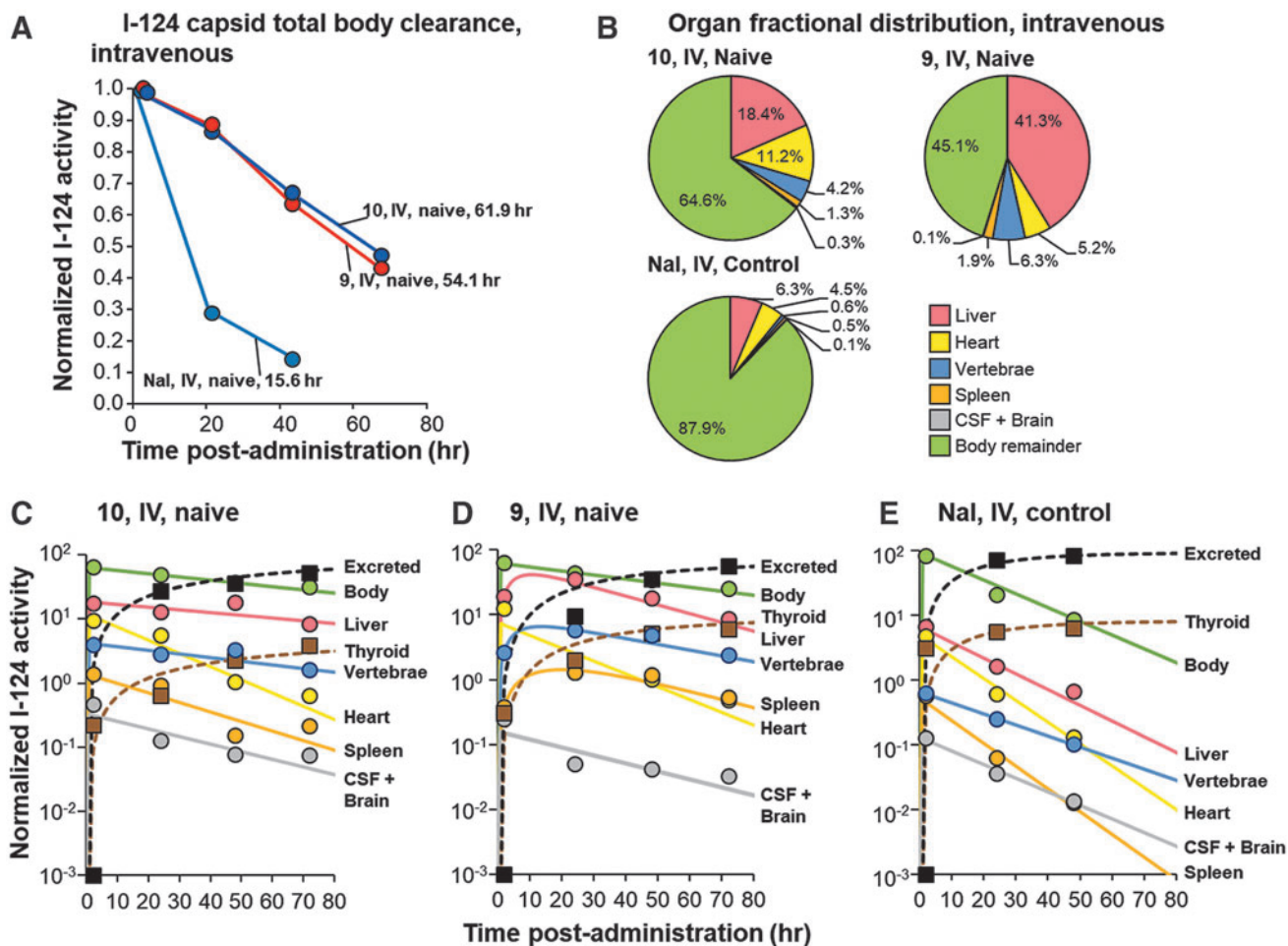


**Figure 2.** Quantification of biodistribution of I-124-labeled AAVrh.10 and AAV9 vectors following intravenous administration to NHP with no preexisting systemic anticapsid immunity. The quantification is based on PET images shown in Fig. 1. **(A)** Whole-body clearance of I-124-labeled AAVrh.10 and AAV9 vectors administered intravenously to NHP1 and NHP2, respectively, with half-lives of AAVrh.10 (61.9 h), AAV9 (54.1 h), and control I-124-Nal (15.6 h). **(B)** Organ fractional distribution (distribution fraction) of I-124-labeled AAVrh.10, AAV9, and Nal, after intravenous administration to NHP1, NHP2, and NHP6, respectively. **(C–E)** Normalized I-124 activity showing uptake and elimination of I-124 in individual organs for AAVrh.10 **(C)**, AAV9 **(D)**, and Nal **(E)** following intravenous administration to capsid immune-naive NHP1, NHP2, and NHP6, respectively. For **(C–E)**, shown is the I-124 relative biodistribution to the liver, vertebrae, heart, spleen, brain/CSF, and body (likely mostly muscle) component. Shown also are thyroid accumulation and calculated excreted I-124. The biological half-life values for each component are detailed in Table 3. CSF, cerebral spinal fluid.

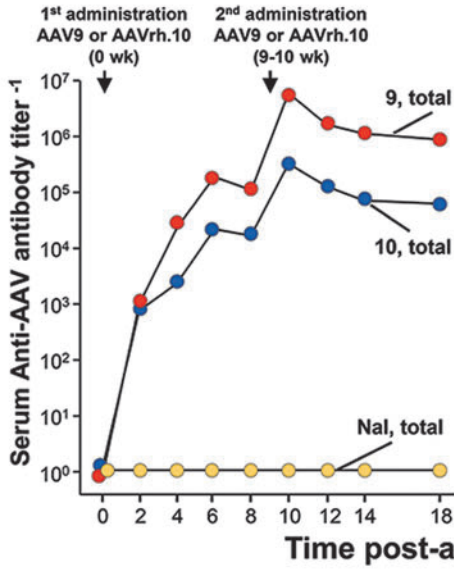
initial distribution of AAV9 versus AAVrh.10, in scans >24 h in the spinal canal (Fig. 5B, C; Supplementary Fig. S4). There was also significant distribution of both vector capsids to the liver. Unexpectedly, however, for the 1–72-h observation period, there was no detectable signal above 1% of the administered amount in the brain

parenchyma. The I-124 signal in the CSF declined over the 72 h, likely representing fragmentation of the capsid and/or removal of the I-124 from the capsid.

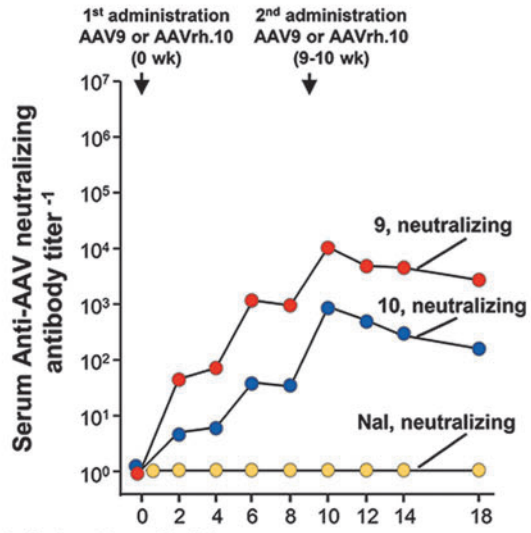
Quantitative analysis demonstrated that the total I-124 body clearance was similar for IC administration of both I-124-AAVrh.10 (84.5 h) and I-124-AAV9 (78.8 h), but

**Figure 3.** Influence of preexisting anticapsid immunity on biodistribution of I-124-labeled AAVrh.10 and AAV9 vectors following intravenous administrations. **(A, B)** Serum anticapsid antibody levels. Capsid immune-naive NHP1 was administered I-124-labeled AAVrh.10mCherry at time 0 (data in Figs. 1 and 2). This evoked total **(A)** and neutralizing **(B)** serum anticapsid antibodies titers. After 9 weeks, NHP1 was administered I-124-labeled AAVrh.10hFXN intravenously to assess the effect of preexisting AAVrh.10 capsid immunity on AAVrh.10 biodistribution as assessed by PET imaging. The same paradigm was used for AAV9 with NHP2, with the first administration of I-124-AAV9mCherry inducing anti-AAV9 antibodies, followed at 10 weeks with the administration of I-124-AAV9hFXN. The Nal control (NHP6) did not have any anti-AAVrh.10 or AAV9 antibodies. For **(C, D)**, the first image is the 1-h image with organs labeled; this is followed by images acquired over time at 24, 48, and 72 h. **(C)** PET images of intravenous administration of I-124-labeled AAVrh.10hFXN administered to NHP1 at 9 weeks when anti-AAVrh.10 systemic immunity had been established. **(D)** PET images of intravenous administration of I-124-labeled AAV9hFXN administered to NHP2 at 10 weeks when anti-AAV9 systemic immunity had been established. All images are maximum intensity projections normalized to injected activity and corrected for physical decay. FXN, frataxin.

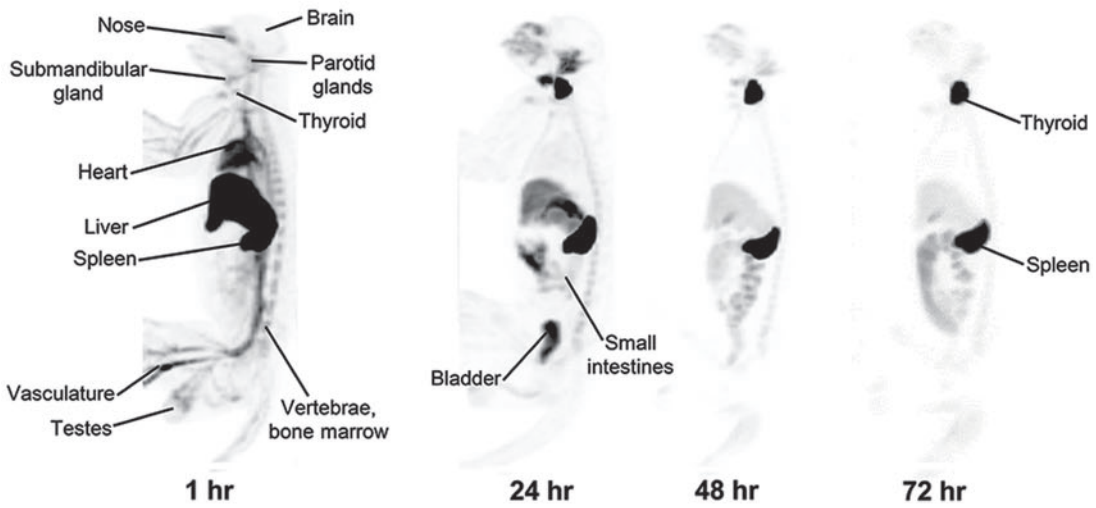
**A Total anti-AAV antibody titers**



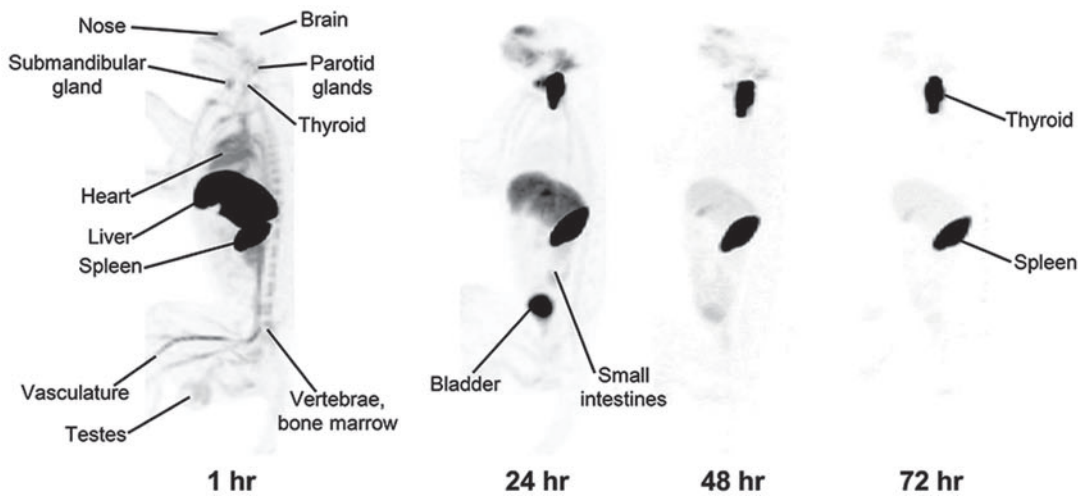
**B Neutralizing anti-AAV antibody titers**



**C Intravenous, AAVrh.10, immune**



**D Intravenous, AAV9, immune**



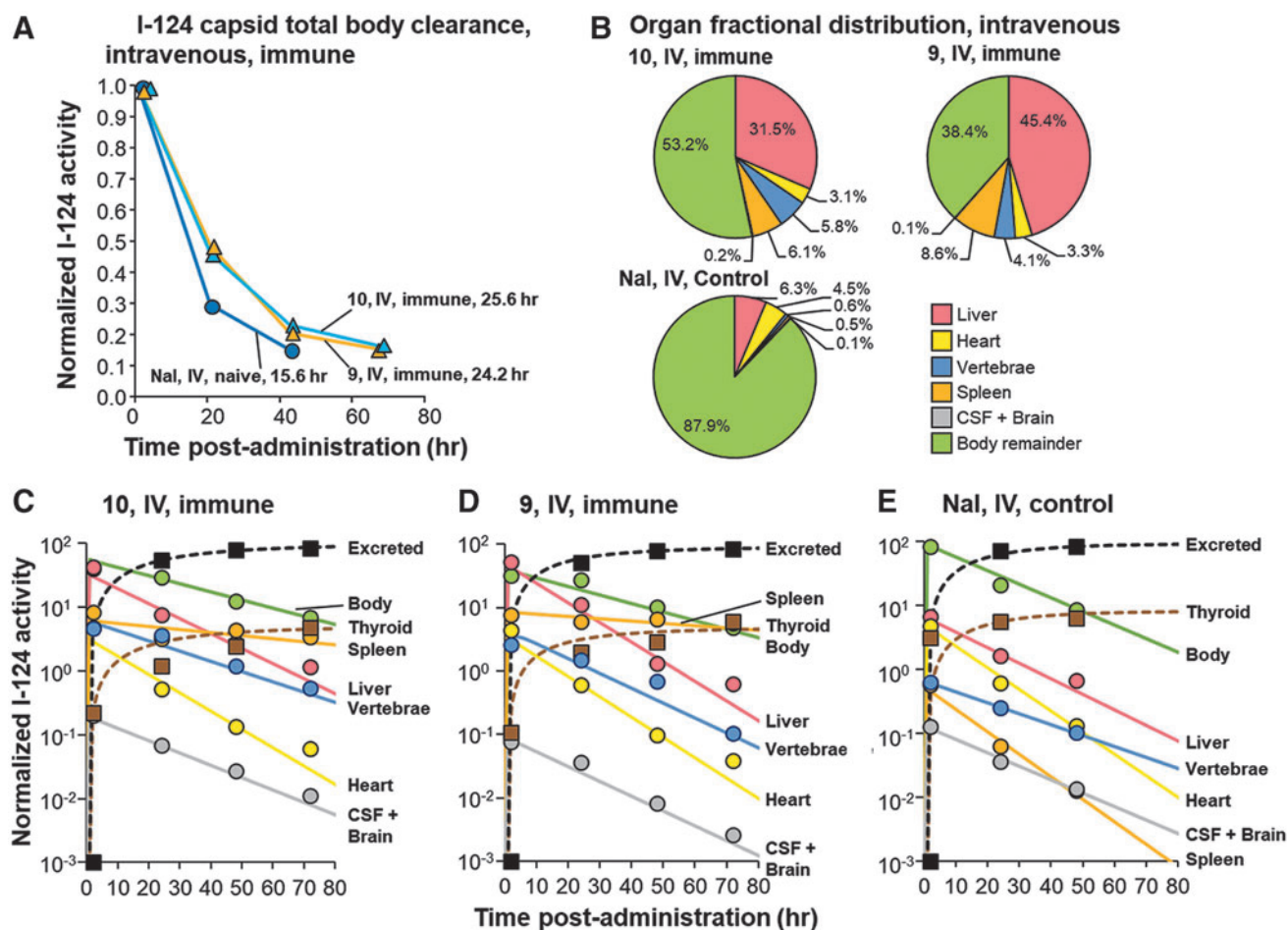


**Figure 4.** Quantification of PET assessment of biodistribution of I-124-labeled AAVrh.10 and AAV9 vectors following repeat intravenous administration to NHP with preexisting anticapsid immunity. The data are derived from quantification of PET studies shown in Fig. 3. **(A)** Whole-body clearance of I-124-labeled AAVrh.10 and AAV9 vectors administered intravenously to vector immune NHP1 and NHP2, respectively, with half-lives of AAVrh.10 (25.6 h) and AAV9 (24.2 h), and 124-NaI (15.6 h) as a control. **(B)** Organ fractional distribution of I-124-labeled AAVrh.10, AAV9, and NaI, after a second intravenous administration to NHP1, NHP2, and NHP6, respectively. **(C–E)** Normalized I-124 activity showing uptake and elimination for individual organs for AAVrh.10 **(C)**, AAV9 **(D)**, and NaI **(E)** following intravenous administration to vector immune NHP1, NHP2, and NHP6, respectively. For **(C–E)**, shown is the I-124 relative biodistribution to the liver, vertebrae, heart, spleen, and brain/CSF. Shown also are the thyroid accumulation and calculated excreted I-124. The biological half-life values for each component are detailed in Table 3.

about 30% slower than the same vectors administered intravenously (compare Fig. 6A with Fig. 2A). Similar to IV administration, the IC organ fractional distribution showed that two-thirds (9) of the vector was widespread in the “body remainder,” that is, not in the CSF, liver, heart, or spleen (Fig. 6B and Table 2), suggesting that despite a local administration to the CSF via the cisterna magna, a significant amount of the labeled vector capsid diffused from the CSF and was distributed throughout the body.

An unexpected finding was that while there was a distribution of 14% (AAVrh.10) and 13% (AAV9) in the CSF, there was again little measurable signal (<1%) in the brain parenchyma, despite direct AAV administration into the CSF via the cisterna magna (Table 2). The  $T_{1/2}$  from the individual organs following IC administration of AAVrh.10 and AAV9 was, in general, similar (Fig. 6 and Table 3).

There is clear evidence from us and others that IC administration of AAVrh.10 and AAV9 vectors to NHP with no preexisting immunity results in effective transfer of vector DNA, mRNA, and protein product throughout the brain.<sup>32,43,48,62–66</sup> Thus, it was an unexpected observation that for the time period assessed (1–72 h), both I-124-AAVrh.10 and I-124-AAV9 vectors administered by the IC route appear to exhibit minimal diffusion into the brain. This observation was even more evident in single slices of brain when compared with the negative NaI control (Fig. 7).

One possibility to explain this discrepancy is that the doses used in the imaging of the immune-naive NHP ( $3.1 \times 10^{12}$  to  $5.7 \times 10^{12}$ ) were too low to saturate possible binding sites, obviating sufficient vector available to enter the CNS and effectively transfect brain cells. In this

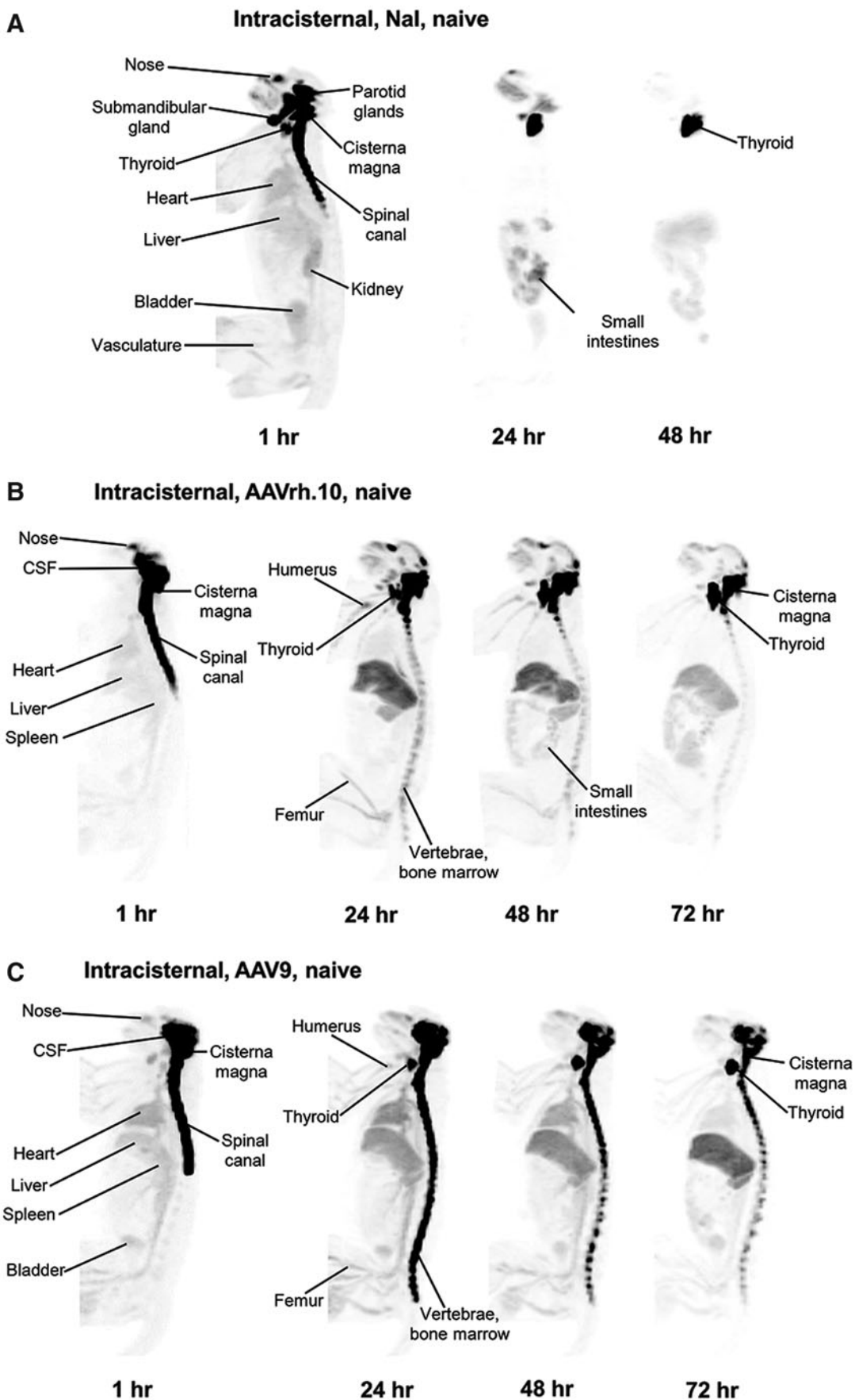


**Figure 5.** PET images of I-124-labeled AAVrh.10 and AAV9 vectors following intracisternal administration. For (A–C), the first image is the 1-h image with identification of positive organs; this is followed by images acquired at 24, 48, and 72 h. See Table 1 for details of the dosing of each NHP. (A) Control intracisternal administration of I-124-labeled Nal alone, vector immune-naive NHP6. (B) Intracisternal administration of I-124-labeled AAVrh.10mCherry, vector immune-naive NHP3. (C) Intracisternal administration of I-124-labeled AAV9mCherry, vector immune-naive NHP4. All images are maximum intensity projections normalized to injected activity and corrected for physical decay.

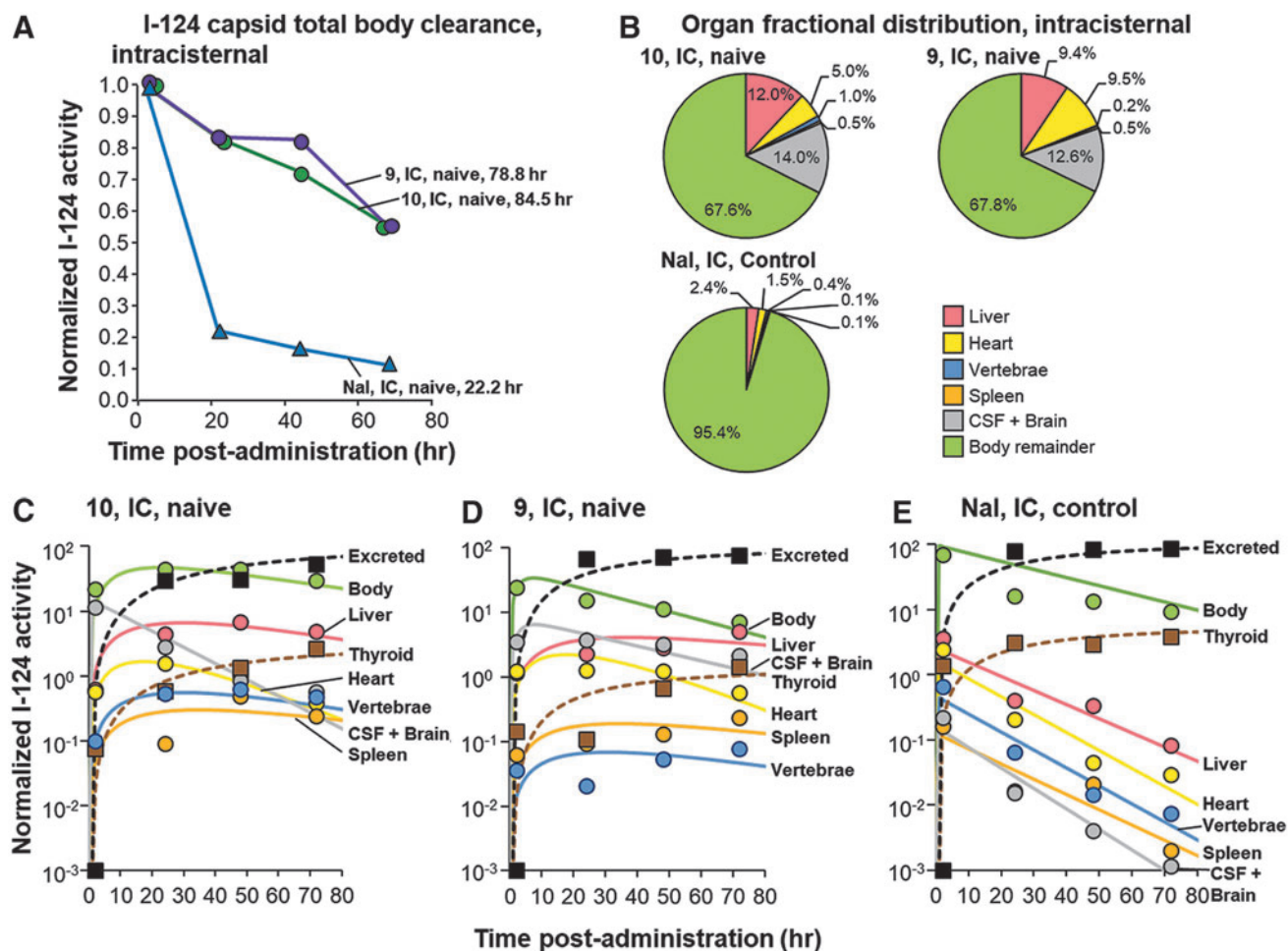


**Figure 6.** Quantification of PET assessment of biodistribution of I-124-labeled AAVrh.10 and AAV9 vectors following intracisternal administration to NHP with no preexisting anticapsid immunity. The data are based on quantification of PET images shown in Fig. 5. **(A)** Whole-body clearance of I-124-labeled AAVrh.10 and AAV9, vectors administered intracisternally to NHP3, NHP4, and NHP6, respectively, with half-lives of AAVrh.10 (84.5 h), AAV9 (78.8 h), and I-124-Nal (22.2 h) as a control. **(B)** Organ fractional distribution of I-124-labeled AAVrh.10, AAV9, and Nal, after intracisternal administration to NHP3, NHP4, and NHP6, respectively. **(C–E)** Normalized I-124 activity showing uptake and elimination for individual organs for AAVrh.10 **(C)**, AAV9 **(D)**, and Nal **(E)** following intracisternal administration to vector-naive NHP3, NHP4, and NHP6, respectively. For **(C–E)**, shown is the I-124 relative biodistribution to the liver, vertebrae, heart, spleen, and brain/CSF. Shown also are the thyroid accumulation and calculated “excreted” I-124. The biological half-life values for each component are detailed in Table 3.

context, the distribution beyond the immediate site of vector deposition might have a threshold such that an initial quantity of vector would be bound and not available for broad distribution. To assess this possibility, we carried out an additional PET study animal (NHP5) in which I-124-labeled-AAV9, with a 10-fold higher total dose ( $5.5 \times 10^{13}$  gc), was administered by the IC route with no preexisting immunity. The pattern of I-124 distribution following IC administration of the 10-fold higher dose at 24 h was generally similar to that of IC administration of I-124-AAV9 with the lower dose (Fig. 8).

Importantly, when the brain of NHP5 was sectioned at 6 weeks after administration, there was widespread expression of the nonsecreted mCherry protein throughout the brain (Fig. 8D), identical to that observed with prior

studies of unlabeled AAV9 and AAVrh.10.<sup>12,28,43</sup> Based on these observations, it is possible that with IC administration, vector slowly diffuses into the CNS over time. Alternatively, the I-124 may be removed from the capsid or the capsid fragments as the virus enters the brain parenchyma. A third possibility is that the observed <1% biodistribution to the brain parenchyma may be correct and is responsible for the amounts of mCherry protein observed.

### IC administration to NHP with preexisting anticapsid immunity

Both NHP responded with anticapsid total and neutralizing antibodies following the first IC administration of I-124-AAVrh.10 and I-124-AAV9 (Fig. 9A, B). When

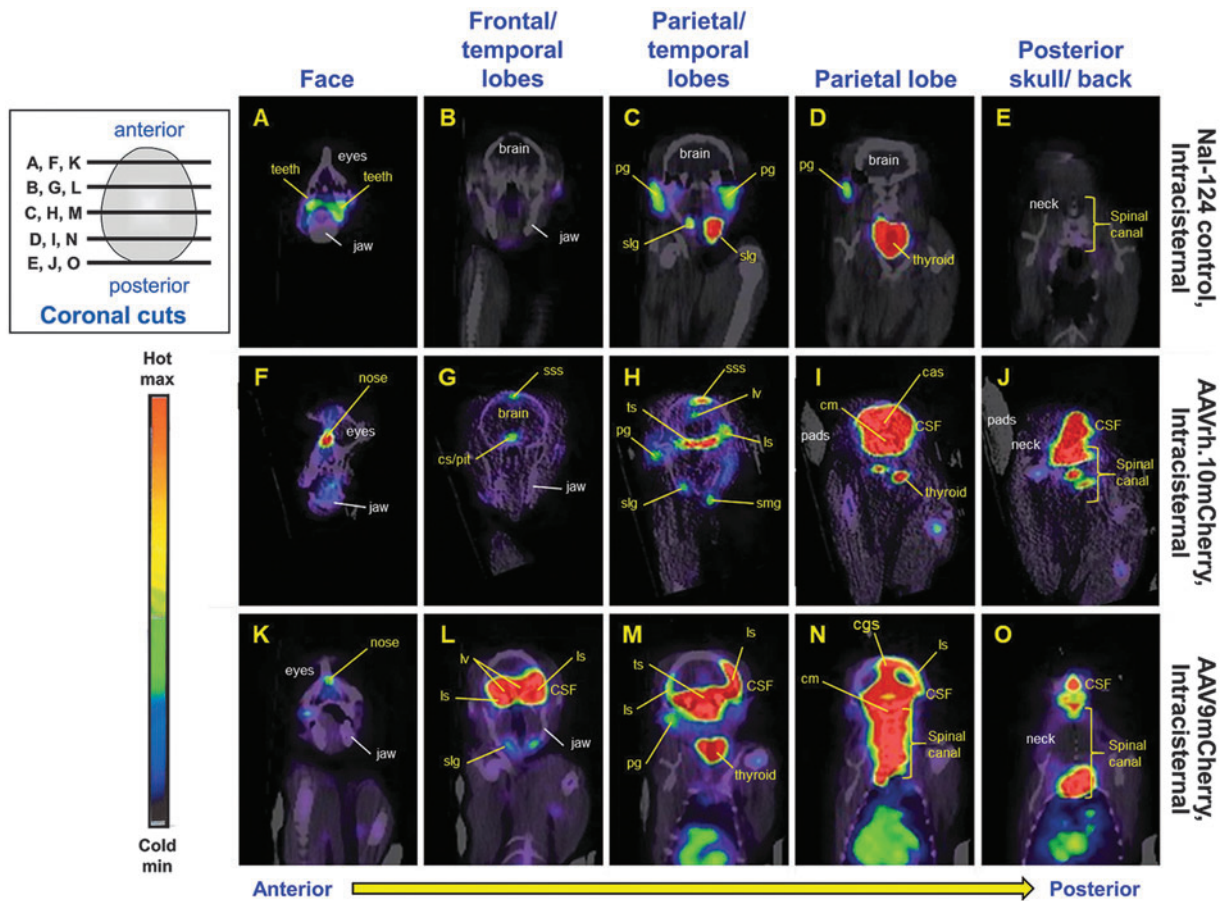


**Figure 7.** PET/CT of I-124-labeled AAVrh.10 and AAV9 vectors in the head region following intracisternal administration to vector immune-naïve NHP. Each NHP PET/CT head was examined using thin cross-sectioning to determine I-124-AAV location 24 h postadministration of I-124-AAV. PET/CT merged sets were sectioned at five representative sites (5 mm thick). See axial view insert for approximate locations of the slices (*black lines* superimposed over the skull), with *panel letters* for each slice. (**A–O**) Each *row* shows five coronal sections, anterior to posterior, for NHP6 (Nal control, **A–E**), NHP3 (AAVrh.10, **F–J**), and NHP4 (AAV9, **K–O**), respectively. The *color bar* shows the intensity of radioactivity for the PET images; identification of I-124 intensity is shown as high I-124 detection in *red/orange*, with lowest *purple/black*. Landmarks in the NHP head and spine are noted in the *panels*, with *white labels* indicating bones and *yellow labels* for I-124 PET signal. Since spatial resolution was limited to a few  $\text{mm}^3$ , it was not always possible to identify specific structures. The top of the skull is at the *top* of each *panel*. The *gray CT shadows* under the head and body are heating pads placed to keep the animals warm during the scans. cas, calcarine sulcus; cgs, cingulate sulcus; cm, cisterna magna; cs, cavernous sinus; CT, computed tomography; ls, lateral sulcus; lv, lateral ventricle; pg, parotid gland; pit, pituitary; slg, sublingual gland; smg, submandibular gland; sss, superior sagittal sinus; ts, transverse sinus.

the I-124-AAVrh.10 and I-124-AAV9 vectors were readministered intracisternally, the preexisting anticapsid immunity had profound effects on the I-124 distribution (Fig. 9C, D). An  $\sim 10$ -fold increase of both I-124-AAVrh.10 and I-124-AAV9 activities was observed in the spleen, similar to IV administration to the immune NHP (Fig. 10 and Table 2). Similar to the IV study, all NHP given a second administration of AAV were monitored by daily observations and biweekly in-life health examinations and blood collection for systemic immunity monitoring (complete blood cell counts and serum chemistry parameters). No adverse events related to the vectors were observed during the study.

In the immune NHP administered with the AAVrh.10 or AAV9 vectors by the IC route, the I-124 total body clearance was rapid (24.4 h for AAVrh.10, 24.5 h for AAV9, close to the total body elimination of the I-124-Nal control;

Fig. 10A). The fractional organ distribution for the immune NHP versus the NHP with no prior anticapsid immunity exhibited an increase in liver distribution and an  $\sim 10$ -fold increase in distribution to the spleen (compare Fig. 10B with Fig. 6B). However, the  $T_{1/2}$  of the I-124 in the individual organs was in general shorter than in the immune-naïve NHP (compare Fig. 10C, D with Fig. 6C, D and Table 3).

### Measurements of I-124 activity and additional compartmental analysis

In most cases, values for I-124 activity obtained from regions-of-interest in the specified organs were  $>10,000$  Bq, yielding a signal-to-noise ratio  $>100:1$ . The main exceptions were in the CSF/brain where some measurements at later time points were as low as 100 Bq for a signal-to-noise ratio of 10:1.

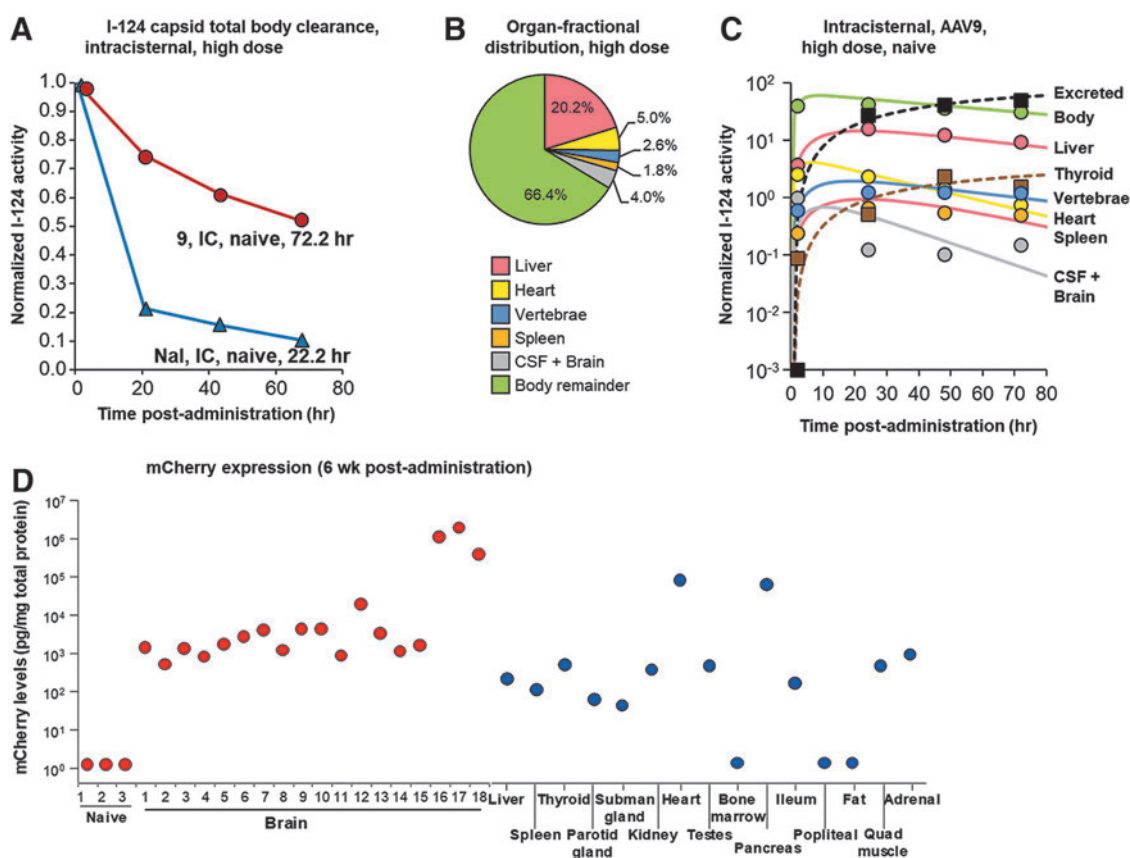


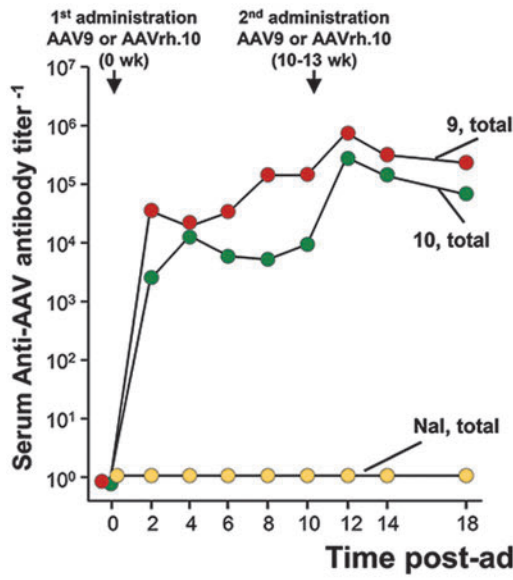
**Figure 8.** Quantification of PET assessment of biodistribution of I-124-labeled AAV9 vectors following intracisternal administration to NHP at high dose with no preexisting anticapsid immunity. **(A)** Whole-body clearance of I-124-labeled AAV9 vectors administered intracisternally to NHP5, with half-lives of AAV9 (72.2 h), and I-124-Nal (22.2 h) as a control. The AAV9mCherry vector was administered at a total dose  $5.5 \times 10^{13}$  gc, see Table 1 for details. **(B)** I-124-capsid total body clearance. **(C)** Organ fractional distribution. **(D)** Normalized I-124 activity showing uptake and elimination for individual organs. **(E)** Biodistribution of mCherry marker protein in brain samples in NHP5 following intracisternal administration of a high dose of AAV9mCherry. mCherry expression was measured throughout the brain and in systemic organs 42 days after intracisternal administration. Following necropsy, the right hemisphere was sectioned into 1-cm-thick coronal slabs and frozen at  $-80^{\circ}\text{C}$ . Separate biopsy punches ( $n=18$ , each 100–200 mg) were taken from across the eight coronal sections to examine biodistribution of vector-mediated mCherry expression. Samples (100–200 mg) were also isolated from various organs to examine systemic mCherry biodistribution. mCherry was quantified by mCherry ELISA; the data are reported as mCherry (pg/mg total protein). Samples from naive NHP that received no AAV were used for negative controls “1–3.” The samples in the NHP5 brain are numbered 1–18: (1) medial orbital gyrus; (2) frontal orbital gyrus; (3) straight gyrus; (4) precentral gyrus; (5) superior frontal gyrus; (6) precentral gyrus; (7) caudate nucleus; (8) precentral gyrus; (9) corpus callosum; (10) thalamus/pars reticulata; (11) superior parietal lobule; (12) pontine nuclei; (13) fusiform gyrus; (14) superior parietal lobule; (15) fusiform gyrus; (16) cerebellum, lobule IV; (17) cerebellum, superior semilunar lobule; and (18) occipital gyrus. The identification of sites was based on [www.scalablebrainatlas.incf.org/macaque](http://www.scalablebrainatlas.incf.org/macaque). ELISA, enzyme-linked immunosorbent assay.

Solutions to the compartmental model of Equation (1) were easily fitted to the organ and sink components (Figs. 2C–E, 4C–E, 6C–E, 8C, and 10C–E), yielding a chi-square per degree-of-freedom of  $1.15 \pm 0.46$  for the full set of 11 experiments listed in Table 1. Only the organs were

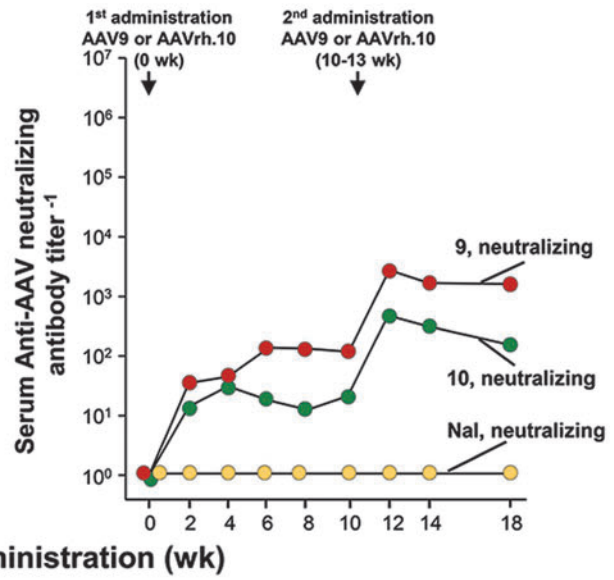
fitted in the initial regression, and the source term  $k_s$  was a parameter of the fitting routine. The half-lives of I-124 from the source were quite similar for all IV administrations ( $0.8 \pm 0.2$  h) as well as for all IC administrations ( $10.4 \pm 3.5$  h; Table 3). In all cases, after leaving the

**Figure 9.** Influence of preexisting anticapsid immunity on biodistribution of I-124-labeled AAVrh.10 and AAV9 vectors following intracisternal administrations. **(A, B)** Serum anticapsid antibody levels. Capsid immune-naive NHP3 was administered I-124-labeled AAVrh.10mCherry at time 0 (data in Figs. 5 and 6). This evoked total **(A)** and neutralizing **(B)** serum anticapsid antibody titers. After 10 weeks, NHP3 was administered I-124-labeled AAVrh.10hFXN by the intracisternal route to assess the effect of preexisting AAVrh.10 capsid immunity on AAVrh.10 biodistribution via PET imaging. The same paradigm was used for AAV9 with NHP4, with the first administration of I-124-AAV9mCherry inducing anti-AAV9 antibodies, followed at 13 weeks with the administration of I-124-AAV9hFXN. The Nal control (NHP6) did not have any anti-AAVrh.10 or AAV9 antibodies. **(C)** PET images of intracisternal administration of I-124-labeled AAVrh.10hFXN administered to NHP3 at 10 weeks when anti-AAVrh.10 systemic immunity had been established. For **(C, D)**, the first image is the 1-h image with organs labeled; this is followed by images acquired over time at 24, 48, and 72 h. **(D)** PET images of intracisternal administration of I-124-labeled AAV9hFXN administered to NHP4 at 13 weeks when anti-AAV9 systemic immunity had been established. All images are maximum intensity projections normalized to injected activity and corrected for physical decay.

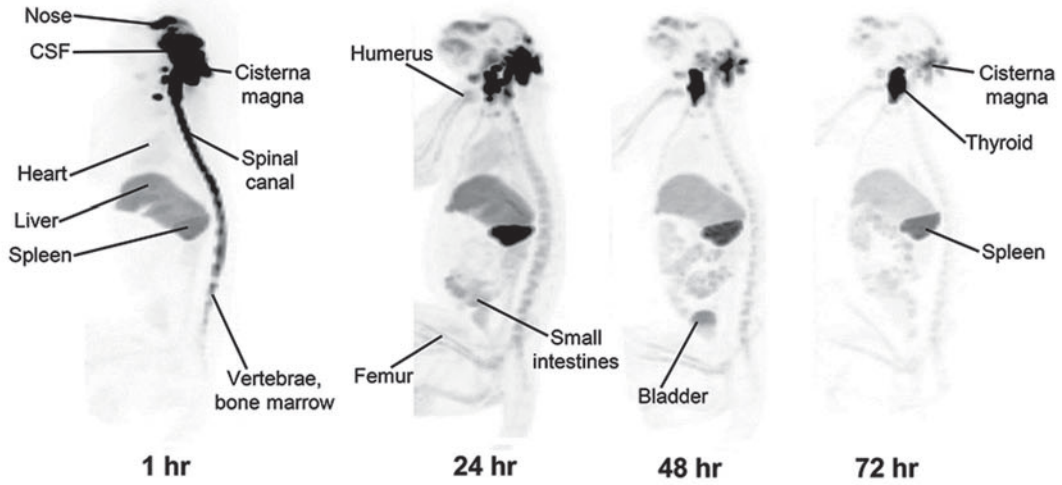
**A Total anti-AAV antibody titers**



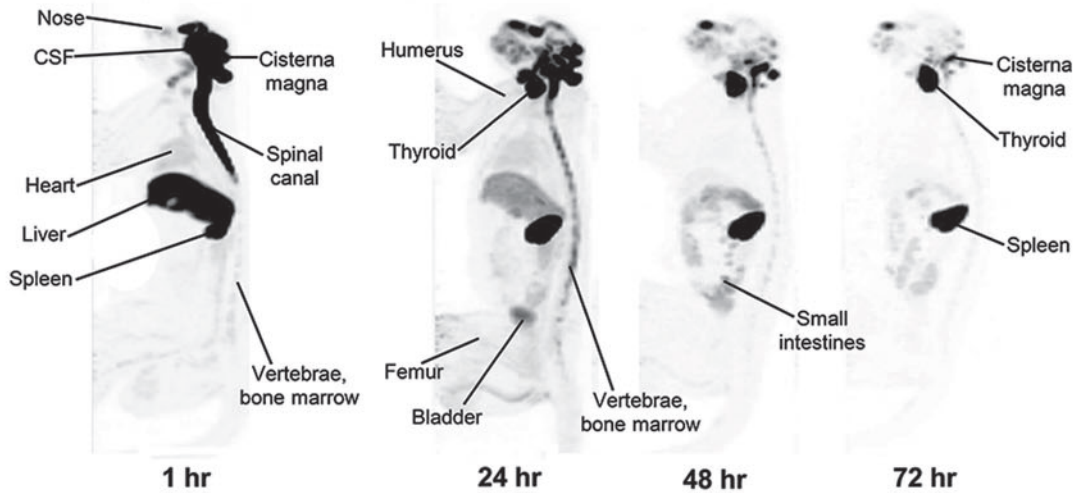
**B Neutralizing anti-AAV antibody titers**



**C Intracisternal, AAVrh.10, immune**



**D Intracisternal, AAV9, immune**



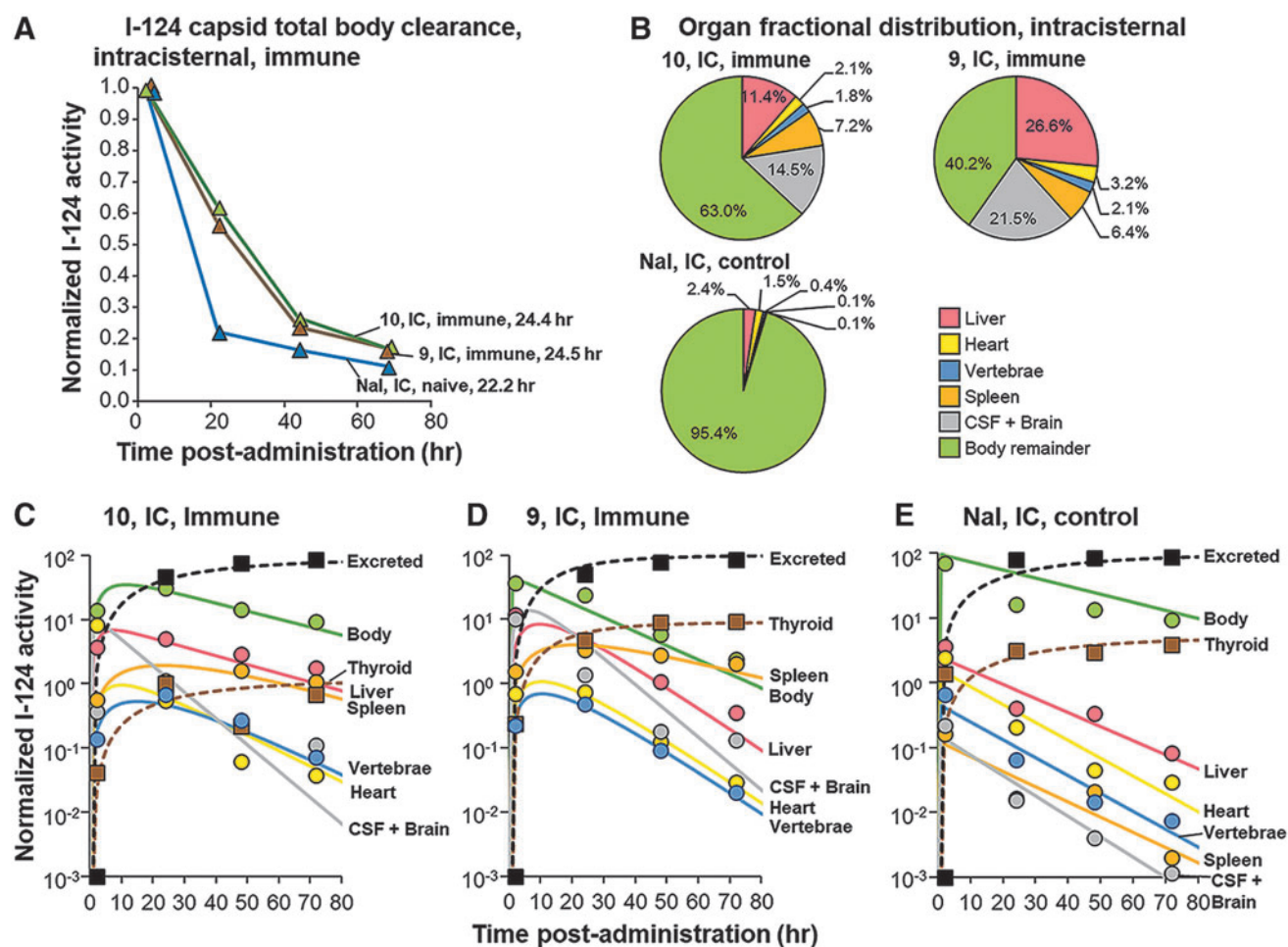


**Figure 10.** Quantification of PET assessment of biodistribution of I-124-labeled AAVrh.10 and AAV9 vectors following repeat intracisternal administration to vector-capsid immune NHP. The data are based on quantification of PET images described in Fig. 9. **(A)** Whole-body clearance of I-124-labeled AAVrh.10 and AAV9 vectors administered by the intracisternal route to vector-immune NHP3 and NHP4, respectively, with half-lives of AAVrh.10 (24.4 h) and AAV9 (24.5 h), and I-124-Nal (22.2 h) as a control. **(B)** Organ fractional distribution of I-124-labeled AAVrh.10, AAV9, and Nal, after a second intracisternal administration to NHP3, NHP4, and NHP6, respectively. **(C–E)** Normalized I-124 activity showing uptake and elimination for individual organs for AAVrh.10 **(C)**, AAV9 **(D)**, and Nal **(E)** following intracisternal administration to vector-immune NHP3, NHP4, and NHP6, respectively. For **(C–E)**, shown is the I-124 relative biodistribution to the liver, vertebrae, heart, spleen, and brain/CSF. Shown also are the thyroid accumulation and calculated excreted I-124. The biological half-life values for each component are detailed in Table 3.

organs, we observed a distribution fraction of only a small percent of I-124 to the thyroid, while the remainder (>95%) was excreted (Figs. 2C–E, 4C–E, 6C–E, 8C, and 10C–E). When the analytical and numerical solutions were compared as a consistency check on the method, there was excellent agreement in all cases.

### Estimates of absolute organ vector doses following administration of I-124-labeled vectors

One important future use of the I-124-labeled capsid technology in humans is that it permits quantification of both the distribution fraction and total vector dose to individual organs, parameters that at present are not available in human trials. In the five NHP, the estimated total vector doses to the major individual organs were obtained

from Equation (3). This result directly depends upon the assumption that, as vector is delivered to its natural targets in the body, I-124 is retained on the capsid. Once the vector is delivered, this assumption no longer applies, as the capsid is processed over time as reflected in the decay constants for each organ.

## DISCUSSION

The gold standard for determining vector biodistribution in experimental animals has been the assessment of vector DNA, mRNA, and/or protein in tissues obtained from euthanized animals.<sup>5,6,19,21–24,60,67,68</sup> Most of these data are in mice,<sup>13,19,69</sup> with limited studies in large animals.<sup>8,17,26–32</sup> Both MRI and PET have been used in mice<sup>25</sup> and NHP<sup>23,52,62,70–76</sup> to image the biodistribution

of vectors and gene products. In humans, there are examples of biodistribution measurements using tissue obtained by biopsy or at autopsy, but there are no systemic noninvasive biodistribution studies of AAV vectors.<sup>33</sup> In addition, to date there has been no quantitative evaluation of vector biodistribution using noninvasive imaging combined with compartmental modeling, which also provides information on the kinetics of vector processing.

We used I-124 labeling of AAVrh.10 and AAV9, and PET combined with a simple compartmental model to assess vector distribution from 1 to 72 h following IV and IC administration to NHP that were naive or immune to the vector capsid. The radioisotope I-124 has been in use for human and animal PET studies for more than many years,<sup>36,77,78</sup> and offers a potential pathway to the use of our methodology to monitor AAV distribution in a clinical setting. Following IV administration, both vectors behaved in a similar manner, distributed primarily to the liver and to a lesser extent heart. Neither was detected at significant levels in the brain. Both vectors administered intravenously also distribute to the vertebrae. Whether this is bone and/or bone marrow is not known, but the observation that the vectors traffic to vertebrae is of interest.<sup>26,27</sup>

Approximately 50% of the labeled capsids were dispersed throughout the body, independent of the liver, heart, and spleen, at least in part in the skeletal muscle. This observation is different from the widespread concept that most intravenously administered vectors distribute primarily to the liver.<sup>21,26,79</sup> Preexisting immunity to the capsid markedly changed the biodistribution, with 10-fold increases in the spleen.

When administered directly to the CSF via the cisterna magna, the I-124-labeled AAV was distributed to organs with a half-life of ~10 h. We know from our prior studies<sup>43</sup> and that of others<sup>32,48,62–66,80</sup> that IC administration of AAVrh.10 and AAV9 vectors is highly effective in transferring to the brain parenchyma vector DNA, with consequent expression of transgene mRNA and protein. In the present study, the one example of NHP5 necropsy showed that widespread expression of the mCherry reporter gene throughout the brain 42 days after IC administration is consistent with prior reports of AAV9 vectors administered by the IC route. It is possible that AAV vectors are bound to receptors in the CSF epithelial lining serving as a source of vector that slowly diffuses into the brain parenchyma. A significant amount of IC-administered vector diffuses out of the CSF (~40–65% of both I-124 AAVrh.10 and I-124 AAV9) and is distributed throughout the body.

The localization of I-124 to the spleen of immunized animals was a consistent finding across both AAV serotypes and both IV and IC delivery routes. The neutralizing titers that were evoked in this study were to mimic the condition of immunity for a readministration of an AAV vector. The prior work of Gray *et al.*<sup>62</sup> showed no inhib-

itory effect of neutralizing titers up to 1:128 at the time of administration. However Samaranch *et al.*<sup>52</sup> showed that neutralizing titers above 1:200 did impact transduction. Therefore, our redistribution of AAV due to immunity with much higher neutralizing titers is consistent with prior published data.

### Assessment of AAV biodistribution using *in vivo* imaging

The concept of using *in vivo* imaging to assess vector biodistribution is not new. For example, optical bioluminescence or fluorescence based on transgene expression, using photons at optical wavelengths, has been used in animal studies.<sup>81–83</sup> However, imaging techniques that rely on reporter genes to measure viral vector biodistribution generally require several days to weeks of delay following administration to generate sufficient expression for evaluation.<sup>21,82,84</sup> Shorter term measurements on the order of a few hours to a few days would facilitate rapid quantification of the relative amount of vector distributed to each organ. In that regard, viral capsid radiolabeling using indium-111<sup>85</sup> and copper-64<sup>25,86</sup> has previously been reported.

In the present study, we made use of available tyrosine residues to bind individual I-124 atoms to the capsid of two serotypes of AAV: AAVrh.10 and AAV9. Given the prevalence of tyrosine residues on capsids of most nonenveloped viruses, this method should have wide applicability. For whole-body measurements of vector biodistribution, PET is a desirable imaging choice because it can scan large fields of view quickly.<sup>87–89</sup> Iodine is attractive not only due to its affinity for binding directly to tyrosine residues on AAV capsid surface proteins, but also since it is a positron emitter with a physical half-life of 4.18 days, detection is possible for several days post-administration.<sup>34</sup>

We therefore focused on the vector distribution during this period (0–72 h). Since the time distribution of the vector varies among the organs, multiple time points were required. The choice of the four time points was selected based upon our previous data in mice<sup>36</sup> and was compatible with the veterinary services required to handle the NHP for imaging. We chose an AAV dose ~ $5 \times 10^{12}$  gc to be administered to the NHP based on the minimal amount that allowed good visualization of the PET signal of I-124 radiolabeled AAV across major organs in the body.

Our methods for capsid radioiodination are applicable to virtually all AAV-based gene therapies. First, since they are independent of transgene, they should be applicable to all AAV serotypes provided the vector has tyrosine residues exposed on the capsid.<sup>37</sup> Second, since our radioiodination methods use I-124, it is suitable for safe and effective translation to humans.<sup>90</sup> I-124 decays, in part, via positron emission, and thus, the ultimate relevant radiations are the 511 keV photons resulting from electron-positron annihilation. Photons of this energy pass easily

through tissue and allow imaging anywhere in the body.<sup>34,36</sup> Third, while the nuclear structure of different iodine isotopes varies, the atomic structure is for our purposes identical. Thus, for example, I-131 could be substituted for I-124, yielding a longer time window for observation, with the caveat that SPECT (single-photon emission computed tomography) must be used rather than PET.

The Iodogen radiolabeling method yielded about two I-124 atoms per capsid on average. We administered to each NHP1–4  $\sim 5 \times 10^{12}$  capsids, which contained on average 390  $\mu\text{Ci}$  of I-124. This permitted high-quality PET images using a vector dose that can be routinely generated in a vector production facility. When compared with an isotope such as carbon-11, which is used routinely in PET studies, I-124 has >300 times the number of nuclei present for the same activity based upon the ratio of the physical half-lives.

### Biodistribution of I-124-labeled capsids

In the present study, imaging of I-124 radioactive decay is proposed as a surrogate for AAV vector biodistribution *in vivo*. While it remains speculative to definitively assign I-124 specifically to labeled virus *in vivo*, absent quantitative data on how I-124 is processed as the capsids are metabolized and transgene activity in each of the studied organs, the compartmental model of Equations (1) is consistent with the following interpretation. First, the organ biodistribution quantification parameters (distribution fractions,  $a_{oi}$ ) describe the affinity of an organ for infection by AAV, while the decay constants ( $k_{oi}$ ) depend upon the dynamics of infection and uncoating. Upon initial vector administration, virtually all I-124 remains bound to the vector in the source compartment, otherwise rapid uptake in the thyroid would be observed, as was observed with the control administration of only I-124 NaI.

Using IV administration of the I-124-labeled AAV, there is very rapid clearance from the blood pool, with a half-life on the order of 1 h, while for IC administration, the half-life is  $\sim 12$  h. Second, I-124 activity in each organ reaches its maximum value rapidly after administration and begins to decline in most organs shortly thereafter, suggesting that receptor binding, translocation, and uncoating processes are underway. Some of the resulting free iodine is taken up by the thyroid, but most I-124 is excreted in the urine or feces, presumably either as free iodine, or bound to capsids or capsid fragments.

Regarding organ biodistribution, the I-124-labeled AAV PET data demonstrate that there is significant distribution to the liver, heart, and vertebrae following both IV and IC administrations of AAV9 and AAVrh.10 to serotype-naïve animals, consistent with previous histopathological studies.<sup>4,26–28</sup> There was a dramatic difference in I-124 distribution in anti-AAV capsid immunized

NHP versus capsid immune-naïve NHP. While also not unexpected, this result can now be quantified, and may be a useful tool for assessing human gene therapy treatment and dosing applications.

There has been considerable interest in AAV9 for CNS applications, with multiple reports of AAV9 effectively crossing the blood/brain barrier following IV administration, including infants with spinal muscular atrophy.<sup>58,91–93</sup> At the IV doses we tested, we observed relatively little I-124 activity in the CNS parenchyma, with values <1% of administered activity in all cases.

In regard to IC administration, cortical brain structures cannot be totally resolved due to the halo effect of I-124 in the CSF surrounding the brain. Thus, it is possible that levels of vector in the cortex were higher than what was measured in deep brain over the 72-h time window of observation. There is also the possibility that vector is quickly dehalogenated on crossing the blood/brain barrier, or that diffusion into the brain parenchyma takes place over a longer timescale than our measurements, and/or that only on the order of up to 1% of vector is delivered to the CNS after IC administration, but this is still sufficient to produce the levels of protein reported in the literature.

One of the limitations of this study is the use of a single NHP for each vector/route of administration/immune status. The use of rodents in this work would have allowed statistical comparisons with larger cohorts per serotype and route of administration. However, NHP afford several significant advantages over rodents. First, the relative PET spatial resolution throughout the whole body is improved since the absolute resolution depends primarily on the positron range and the size of the 511 keV photon detectors. Second, organ vector tropism in NHP more closely approximates humans. Third, an animal model with a large brain size with physiology and biochemistry as close as possible to that of the human is needed to infer dosing for future clinical usage.<sup>94</sup>

The size of the NHP brain is  $\sim 80$  g compared with 2 g for the rat brain<sup>43,95</sup>; therefore, vector diffusion through the brain is much more indicative of what may be expected in the 700 g human brain. The intermediate brain size also allows for a smaller dose scale up to human, 10-fold, rather than 500–1,000 $\times$  for rodents to human. The challenge to using NHP is the expense related to purchase and housing, as well as management throughout the experimental procedures, which required significant veterinary support. Since all experiments were performed with  $n=1$  animal per serotype and delivery route, the imaging and dosimetry results should be considered to be preliminary.

### Advantages and challenges of I-124 AAV capsid labeling and imaging

As demonstrated, this technology facilitates the introduction of *in vivo* viral vector organ dosimetry, and the

simple compartmental model presented is a first step toward this goal. Further refinement of this concept requires additional consideration of both physical and biological processes affecting the observed I-124 signal. Physical processes include all of the variables that enter into calculations to convert the detection of electron-positron annihilations in a PET scanner into the spatial and temporal distribution of activity. Biological mechanisms include initial vector distribution in the source pool, followed by vector uptake and uncoating, as well as removal and secretion of intact vector or vector fragments. While the present study focused on PET imaging, the measurement of urine and blood for AAV intact capsids versus capsid fragments would add important information to the mechanisms behind AAV kinetics.

A limitation of this study is that there was no quantitative whole-body method available for comparison of biodistribution with the transgene product at a spatial resolution similar to PET. Optical imaging of fluorescent reporter genes offers visual confirmation of successful infection and transduction in any organ, but currently can provide only qualitative information regarding biodistribution. Additional development of quantitative noninvasive biomarkers for transgene biodistribution will be useful.

Noninvasive methods to map AAV vector biodistribution throughout the body are useful not only to identify capsid fate but also to identify off-target biodistribution for potential vector toxicity.<sup>3</sup> The radiolabeling method chosen preserves significant vector function,<sup>37</sup> and PET provides a platform for quantitative assessment of vector biodistribution. After refinement of our radiochemistry procedures to consistently produce several 100  $\mu$ Ci of labeled product containing  $>10^{12}$  AAV capsids, infectivity assays consistently yielded about 60% versus unlabeled virus activity per 10,000 genome copies per cell.<sup>37</sup> Both the radiochemistry and imaging methods were designed to facilitate noninvasive imaging well-suited for ultimate translation to human use.

A direct benefit of the methodology would be the ability to noninvasively monitor the effectiveness of AAV vector administration in AAV gene therapy trials.<sup>96</sup> This should

aid rapid assessment of new capsid designs and different delivery routes by providing specific knowledge regarding organ tropism in humans.

In conclusion, AAV capsids are amenable to stable radioiodination based upon numerous exposed tyrosine surface residues. The radiochemical method and resulting labeling efficiency allow visualization and quantitation of organ biodistribution via PET imaging after vector administration. The methods described in this study have significant translation potential to humans and are transgene independent, suggesting their utility in a wide range of gene therapy applications, where they should facilitate the selection of appropriate delivery routes, vector doses, and evaluation of potential toxicity for both novel and existing vector serotypes and capsid designs.<sup>97</sup> A natural outgrowth of this technology is the development of quantitative viral vector dosimetry, which should aid in unblinding gene therapy administration and contributing to precision medicine in the field.

## ACKNOWLEDGMENTS

We thank Nahla Mohamed for editorial help and Simon Morim for assistance in the PET/CT imaging.

## AUTHOR DISCLOSURE

D.J.B., R.G.C., S.M.K., P.K., B.P.D., D.S., and J.B. have a relevant patent pending.

## FUNDING INFORMATION

This work was funded, in part, by REGENXBIO; NIH EB027918; and the Departments of Genetic Medicine and Radiology.

## SUPPLEMENTARY MATERIAL

Supplementary Figure 1  
Supplementary Figure 2  
Supplementary Figure 3  
Supplementary Figure 4  
Supplementary Video 1  
Supplementary Video 2

## REFERENCES

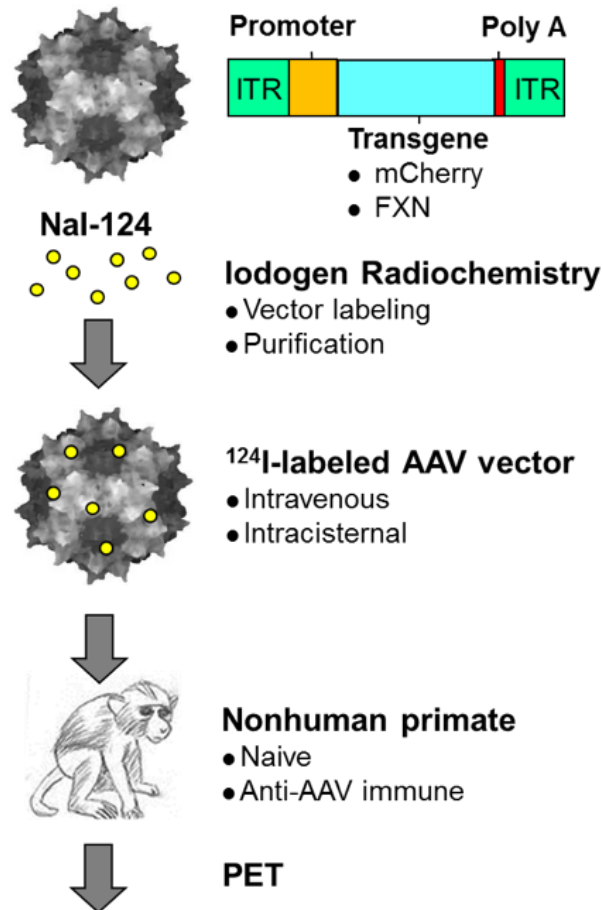
- White MD, Milne RV, Nolan MF. A molecular toolbox for rapid generation of viral vectors to up- or down-regulate neuronal gene expression in vivo. *Front Mol Neurosci* 2011;4:8.
- Balakrishnan B, Jayandharan GR. Basic biology of adeno-associated virus (AAV) vectors used in gene therapy. *Curr Gene Ther* 2014;14:86–100.
- Colella P, Ronzitti G, Mingozzi F. Emerging issues in AAV-mediated in vivo gene therapy. *Mol Ther Methods Clin Dev* 2018;8:87–104.
- Gao G, Vandenberghe LH, Alvira MR, et al. Clades of adeno-associated viruses are widely disseminated in human tissues. *J Virol* 2004;78:6381–6388.
- Hocquemiller M, Giersch L, Audrain M, et al. Adeno-associated virus-based gene therapy for CNS diseases. *Hum Gene Ther* 2016;27:478–496.
- Naso MF, Tomkowicz B, Perry WL, III et al. Adeno-associated virus (AAV) as a vector for gene therapy. *BioDrugs* 2017;31:317–334.
- Carter BJ. Adeno-associated virus and the development of adeno-associated virus vectors: a historical perspective. *Mol Ther* 2004;10:981–989.
- Herzog CD, Bishop KM, Brown L, et al. Gene transfer provides a practical means for safe, long-term, targeted delivery of biologically active neurotrophic factor proteins for neurodegenerative diseases. *Drug Deliv Transl Res* 2011;1:361–382.
- Nathwani AC, Tuddenham EG, Rangarajan S, et al. Adenovirus-associated virus vector-mediated gene transfer in hemophilia B. *N Engl J Med* 2011;365:2357–2365.
- Bennett J, Wellman J, Marshall KA, et al. Safety and durability of effect of contralateral-eye administration of AAV2 gene therapy in patients with childhood-onset blindness caused by RPE65 mutations: a follow-on phase 1 trial. *Lancet* 2016;388:661–672.
- Chiuchiolio MJ, Kaminsky SM, Sondhi D, et al. Intrapleural administration of an AAVrh.10 vector coding for human alpha1-antitrypsin for the treatment of alpha1-antitrypsin deficiency. *Hum Gene Ther Clin Dev* 2013;24:161–173.
- Rosenberg JB, Sondhi D, Rubin DG, et al. Comparative efficacy and safety of multiple routes of direct CNS administration of adeno-associated virus gene transfer vector serotype rh.10 expressing the human arylsulfatase A cDNA to nonhuman primates. *Hum Gene Ther Clin Dev* 2014;25:164–177.
- Aschauer DF, Kreuz S, Rumpel S. Analysis of transduction efficiency, tropism and axonal transport of AAV serotypes 1, 2, 5, 6, 8 and 9 in the mouse brain. *PLoS One* 2013;8:e76310.
- Gao G, Vandenberghe LH, Wilson JM. New recombinant serotypes of AAV vectors. *Curr Gene Ther* 2005;5:285–297.
- Cearley CN, Wolfe JH. Transduction characteristics of adeno-associated virus vectors expressing cap serotypes 7, 8, 9, and Rh10 in the mouse brain. *Mol Ther* 2006;13:528–537.
- Vandenberghe LH, Wilson JM, Gao G. Tailoring the AAV vector capsid for gene therapy. *Gene Ther* 2009;16:311–319.
- Salegio EA, Kells AP, Richardson RM, et al. Magnetic resonance imaging-guided delivery of adeno-associated virus type 2 to the primate brain for the treatment of lysosomal storage disorders. *Hum Gene Ther* 2010;21:1093–1103.
- Asokan A, Schaffer DV, Samulski RJ. The AAV vector toolkit: poised at the clinical crossroads. *Mol Ther* 2012;20:699–708.
- Ling C, Wang Y, Zhang Y, et al. Selective in vivo targeting of human liver tumors by optimized AAV3 vectors in a murine xenograft model. *Hum Gene Ther* 2014;25:1023–1034.
- Hudry E, Vandenberghe LH. Therapeutic AAV gene transfer to the nervous system: a clinical reality. *Neuron* 2019;101:839–862.
- Zincarelli C, Soltys S, Rengo G, et al. Analysis of AAV serotypes 1–9 mediated gene expression and tropism in mice after systemic injection. *Mol Ther* 2008;16:1073–1080.
- Choudhury SR, Hudry E, Maguire CA, et al. Viral vectors for therapy of neurologic diseases. *Neuropharmacology* 2017;120:63–80.
- Cunningham J, Pivrotto P, Bringas J, et al. Biodistribution of adeno-associated virus type-2 in nonhuman primates after convection-enhanced delivery to brain. *Mol Ther* 2008;16:1267–1275.
- Schuster DJ, Dykstra JA, Riedl MS, et al. Biodistribution of adeno-associated virus serotype 9 (AAV9) vector after intrathecal and intravenous delivery in mouse. *Front Neuroanat* 2014;8:42.
- Seo JW, Ingham ES, Mahakian L, et al. Positron emission tomography imaging of novel AAV capsids maps rapid brain accumulation. *Nat Commun* 2020;11:2102.
- Gao G, Lu Y, Calcedo R, et al. Biology of AAV serotype vectors in liver-directed gene transfer to nonhuman primates. *Mol Ther* 2006;13:77–87.
- Nathwani AC, Rosales C, McIntosh J, et al. Long-term safety and efficacy following systemic administration of a self-complementary AAV vector encoding human FIX pseudotyped with serotype 5 and 8 capsid proteins. *Mol Ther* 2011;19:876–885.
- Hinderer C, Bell P, Gurda BL, et al. Intrathecal gene therapy corrects CNS pathology in a feline model of mucopolysaccharidosis I. *Mol Ther* 2014;22:2018–2027.
- Samaranch L, Sebastian WS, Kells AP, et al. AAV9-mediated expression of a non-self protein in nonhuman primate central nervous system triggers widespread neuroinflammation driven by antigen-presenting cell transduction. *Mol Ther* 2014;22:329–337.
- Yang B, Li S, Wang H, et al. Global CNS transduction of adult mice by intravenously delivered rAAVrh.8 and rAAVrh.10 and nonhuman primates by rAAVrh.10. *Mol Ther* 2014;22:1299–1309.
- Hocquemiller M, Hemsley KM, Douglass ML, et al. AAVrh10 vector corrects disease pathology in MPS IIIA mice and achieves widespread distribution of SGSH in large animal brains. *Mol Ther Methods Clin Dev* 2020;17:174–187.
- Hordeaux J, Hinderer C, Buza EL, et al. Safe and sustained expression of human iduronidase after intrathecal administration of adeno-associated virus serotype 9 in infant rhesus monkeys. *Hum Gene Ther* 2019;30:957–966.
- Manno CS, Chew AJ, Hutchison S, et al. AAV-mediated factor IX gene transfer to skeletal muscle in patients with severe hemophilia B. *Blood* 2003;101:2963–2972.
- Koehler L, Gagnon K, McQuarrie S, et al. Iodine-124: a promising positron emitter for organic PET chemistry. *Molecules* 2010;15:2686–2718.
- Cascini GL, Niccoli Asabella A, Notaristefano A, et al. 124 Iodine: a longer-life positron emitter isotope-new opportunities in molecular imaging. *Biomed Res Int* 2014;2014:672094.
- Kuker R, Stzjenberg M, Gulec S. I-124 imaging and dosimetry. *Mol Imaging Radionucl Ther* 2017;26:66–73.
- Kothari P, De BP, He B, et al. Radioiodinated capsids facilitate in vivo non-invasive tracking of adeno-associated gene transfer vectors. *Sci Rep* 2017;7:39594.
- Ballon D, Rosenberg JB, Kothari P, et al. Whole-body imaging of adeno-associated viral vector biodistribution in non-human primates. *Mol Ther* 2019;27(Suppl 1):230.
- Fan JY, Cui ZQ, Wei HP, et al. Split mCherry as a new red bimolecular fluorescence complementation system for visualizing protein-protein interactions in living cells. *Biochem Biophys Res Commun* 2008;367:47–53.
- De BP, Heguy A, Hackett NR, et al. High levels of persistent expression of alpha1-antitrypsin mediated by the nonhuman primate serotype rh.10 adeno-associated virus despite preexisting immunity to common human adeno-associated viruses. *Mol Ther* 2006;13:67–76.
- Sondhi D, Peterson DA, Giannaris EL, et al. AAV2-mediated CLN2 gene transfer to rodent and nonhuman primate brain results in long-term TPP-I expression compatible with therapy for LINCL. *Gene Ther* 2005;12:1618–1632.
- Zerah M, Piguet F, Colle MA, et al. Intracerebral gene therapy using AAVrh.10-hARSA recombinant vector to treat patients with early-onset forms of metachromatic leukodystrophy: preclinical feasibility and safety assessments in nonhuman primates. *Hum Gene Ther Clin Dev* 2015;26:113–124.
- Rosenberg JB, Kaplitt MG, De BP, et al. AAVrh.10-mediated APOE2 central nervous system gene therapy for APOE4-associated Alzheimer's disease. *Hum Gene Ther Clin Dev* 2018;29:24–47.

44. Sondhi D, Rosenberg JB, De BP, et al. Long-term toxicology evaluation of AAVrh.10hARSA administration to the CNS of nonhuman primates to treat metachromatic leukodystrophy. *Mol Ther* 2016;44:S146.
45. Bailey GS. The Iodogen method for radiolabeling protein. In: Walker JM, ed. *The Protein Protocols Handbook*. Totowa, NJ: Humana Press, 1996:673–674.
46. Sondhi D, Johnson L, Purpura K, et al. Long-term expression and safety of administration of AAVrh.10hCLN2 to the brain of rats and nonhuman primates for the treatment of late infantile neuronal ceroid lipofuscinosis. *Hum Gene Ther Methods* 2012;23:324–335.
47. Hackett NR, Redmond DE, Sondhi D, et al. Safety of direct administration of AAV2(CU)hCLN2, a candidate treatment for the central nervous system manifestations of late infantile neuronal ceroid lipofuscinosis, to the brain of rats and nonhuman primates. *Hum Gene Ther* 2005;16:1484–1503.
48. Hardcastle N, Boulis NM, Federici T. AAV gene delivery to the spinal cord: serotypes, methods, candidate diseases, and clinical trials. *Expert Opin Biol Ther* 2018;18:293–307.
49. Bevan AK, Duque S, Foust KD, et al. Systemic gene delivery in large species for targeting spinal cord, brain, and peripheral tissues for pediatric disorders. *Mol Ther* 2011;19:1971–1980.
50. Hinderer C, Bell P, Katz N, et al. Evaluation of intrathecal routes of administration for adeno-associated viral vectors in large animals. *Hum Gene Ther* 2018;29:15–24.
51. Meyer K, Ferraiuolo L, Schmelzer L, et al. Improving single injection CSF delivery of AAV9-mediated gene therapy for SMA: a dose-response study in mice and nonhuman primates. *Mol Ther* 2015;23:477–487.
52. Samaranch L, Salegio EA, San Sebastian W, et al. Adeno-associated virus serotype 9 transduction in the central nervous system of nonhuman primates. *Hum Gene Ther* 2012;23:382–389.
53. Lubberink M, Herzog H. Quantitative imaging of 124I and 86Y with PET. *Eur J Nucl Med Mol Imaging* 2011;38(Suppl 1):S10–S18.
54. Rausch I, Cal-Gonzalez J, Dapra D, et al. Performance evaluation of the Biograph mCT Flow PET/CT system according to the NEMA NU2–2012 standard. *EJNMMI Phys* 2015;2:26.
55. Lee YS, Kim JS, Kim JY, et al. Spatial resolution and image qualities of Zr-89 on Siemens Biograph TruePoint PET/CT. *Cancer Biother Radiopharm* 2015;30:27–32.
56. Lee YS, Kim JS, Kim HJ, et al. Imaging characteristics of 124I between 3D and 2D on siemens ECAT HR+PET scanner. *IEEE Trans Nucl Sci* 2013;60.
57. Boyce WE, DiPrima RC. Systems of first order linear equations. In: *Elementary Differential Equations*. Hoboken, NJ: Wiley, 2012:359–449.
58. Mendell JR, Al-Zaidy S, Shell R, et al. Single-dose gene-replacement therapy for spinal muscular atrophy. *N Engl J Med* 2017;377:1713–1722.
59. Shephard GS, Thiel PG, Sydenham EW, et al. Fate of a single dose of 14C-labelled fumonisins B1 in vervet monkeys. *Nat Toxins* 1995;3:145–150.
60. Mori S, Takeuchi T, Enomoto Y, et al. Biodistribution of a low dose of intravenously administered AAV-2, 10, and 11 vectors to cynomolgus monkeys. *Jpn J Infect Dis* 2006;59:285–293.
61. Grand TI. Body weight: its relation to tissue composition, segment distribution, and motor function. I. Interspecific comparisons. *Am J Phys Anthropol* 1977;47:211–240.
62. Gray SJ, Nagabushan Kalburgi S, McCown TJ, et al. Global CNS gene delivery and evasion of anti-AAV-neutralizing antibodies by intrathecal AAV administration in non-human primates. *Gene Ther* 2013;20:450–459.
63. Samaranch L, Salegio EA, San Sebastian W, et al. Strong cortical and spinal cord transduction after AAV7 and AAV9 delivery into the cerebrospinal fluid of nonhuman primates. *Hum Gene Ther* 2013;24:526–532.
64. Bucher T, Colle MA, Wakeling E, et al. scAAV9 intracisternal delivery results in efficient gene transfer to the central nervous system of a feline model of motor neuron disease. *Hum Gene Ther* 2013;24:670–682.
65. Bucher T, Dubreil L, Colle MA, et al. Intracisternal delivery of AAV9 results in oligodendrocyte and motor neuron transduction in the whole central nervous system of cats. *Gene Ther* 2014;21:522–528.
66. Hordeaux J, Yuan Y, Clark PM, et al. The GPI-linked protein LY6A drives AAV-PHP.B transport across the blood-brain barrier. *Mol Ther* 2019;27:912–921.
67. Marsic D, Mendez-Gomez HR, Zolotukhin S. High-accuracy biodistribution analysis of adeno-associated virus variants by double barcode sequencing. *Mol Ther Methods Clin Dev* 2015;2:15041.
68. Zhou X, Shen L, Liu L, et al. Preclinical safety evaluation of recombinant adeno-associated virus 2 vector encoding human tumor necrosis factor receptor-immunoglobulin Fc fusion gene. *Hum Vaccin Immunother* 2016;12:732–739.
69. Buning H, Srivastava A. Capsid modifications for targeting and improving the efficacy of AAV vectors. *Mol Ther Methods Clin Dev* 2019;12:248–265.
70. Nathwani AC, Gray JT, McIntosh J, et al. Safe and efficient transduction of the liver after peripheral vein infusion of self-complementary AAV vector results in stable therapeutic expression of human FIX in nonhuman primates. *Blood* 2007;109:1414–1421.
71. Aalbers CJ, Bevaart L, Loiler S, et al. Preclinical potency and biodistribution studies of an AAV 5 vector expressing human interferon-beta (ART-I02) for local treatment of patients with rheumatoid arthritis. *PLoS One* 2015;10:e0130612.
72. Majowicz A, Salas D, Zabaleta N, et al. Successful repeated hepatic gene delivery in mice and non-human primates achieved by sequential administration of AAV5(ch) and AAV1. *Mol Ther* 2017;25:1831–1842.
73. Seitz IP, Michalakos S, Wilhelm B, et al. Superior retinal gene transfer and biodistribution profile of subretinal versus intravitreal delivery of AAV8 in nonhuman primates. *Invest Ophthalmol Vis Sci* 2017;58:5792–5801.
74. Liguore WA, Domire JS, Button D, et al. AAV-PHP.B administration results in a differential pattern of CNS biodistribution in non-human primates compared with mice. *Mol Ther* 2019;27:2018–2037.
75. Ohno K, Samaranch L, Hadaczek P, et al. Kinetics and MR-based monitoring of AAV9 vector delivery into cerebrospinal fluid of nonhuman primates. *Mol Ther Methods Clin Dev* 2019;13:47–54.
76. Bey K, Deniaud J, Dubreil L, et al. Intra-CSF AAV9 and AAVrh10 administration in nonhuman primates: promising routes and vectors for which neurological diseases? *Mol Ther Methods Clin Dev* 2020;17:771–784.
77. Pentlow KS, Graham MC, Lambrecht RM, et al. Quantitative imaging of iodine-124 with PET. *J Nucl Med* 1996;37:1557–1562.
78. Grewal RK, Lubberink M, Pentlow KS, et al. The role of iodine-124-positron emission tomography imaging in the management of patients with thyroid cancer. *PET Clin* 2007;2:313–320.
79. Baruteau J, Waddington SN, Alexander IE, et al. Delivering efficient liver-directed AAV-mediated gene therapy. *Gene Ther* 2017;24:263–264.
80. Hordeaux J, Dubreil L, Deniaud J, et al. Efficient central nervous system AAVrh10-mediated intrathecal gene transfer in adult and neonate rats. *Gene Ther* 2015;22:316–324.
81. Herve J, Cunha AS, Liu B, et al. Recombinant viral vectors expressing sodium-iodide symporter for hepatocellular carcinoma radiotherapy. *J Hepatol* 2006;44:S143–S144.
82. Moulay G, Ohtani T, Ogut O, et al. Cardiac AAV9 gene delivery strategies in adult canines: assessment by long-term serial SPECT imaging of sodium iodide symporter expression. *Mol Ther* 2015;23:1211–1221.
83. Pham L, Suksanpaisan L, Peng KW, et al. Longitudinal high resolution 3-D imaging of AAV gene expression in vivo. *Mol Ther* 2015;23:S221.
84. Haywood T, Beinat C, Gowrishankar G, et al. Positron emission tomography reporter gene strategy for use in the central nervous system. *Proc Natl Acad Sci U S A* 2019;116:11402–11407.
85. Schellingerhout D, Rainov NG, Breakefield XO, et al. Quantitation of HSV mass distribution in a rodent brain tumor model. *Gene Ther* 2000;7:1648–1655.

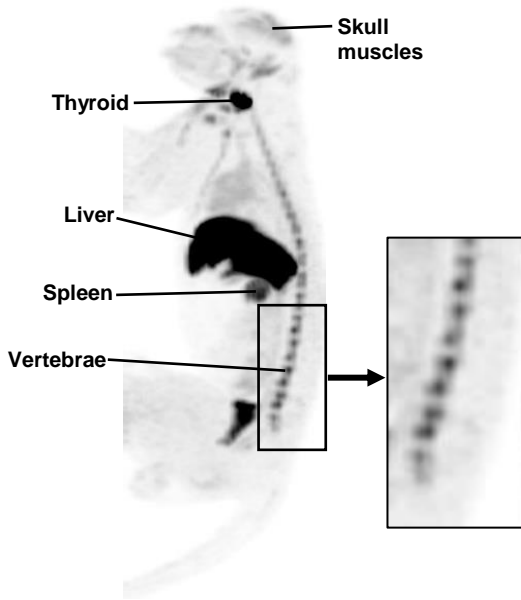
86. Farkas ME, Aanei IL, Behrens CR, et al. PET Imaging and biodistribution of chemically modified bacteriophage MS2. *Mol Pharm* 2013;10:69–76.
87. Jones T, Townsend D. History and future technical innovation in positron emission tomography. *J Med Imaging (Bellingham)* 2017;4:011013.
88. Cherry SR, Jones T, Karp JS, et al. Total-body PET: maximizing sensitivity to create new opportunities for clinical research and patient care. *J Nucl Med* 2018;59:3–12.
89. Papisov M, Belov V. Chapter 13—solute transport in the cerebrospinal fluid: physiology and practical implications. In: Lonser RR, Sarntinoranont M, Bankiewicz K, eds. *Nervous System Drug Delivery*. Cambridge, MA: Academic Press, Elsevier, 2019: 251–274.
90. Behr TM, Gotthardt M, Becker W, et al. Radioiodination of monoclonal antibodies, proteins and peptides for diagnosis and therapy. A review of standardized, reliable and safe procedures for clinical grade levels kBq to GBq in the Gottingen/Marburg experience. *Nuklearmedizin* 2002;41:71–79.
91. Duque S, Joussemet B, Riviere C, et al. Intravenous administration of self-complementary AAV9 enables transgene delivery to adult motor neurons. *Mol Ther* 2009;17:1187–1196.
92. Yamashita T, Chai HL, Teramoto S, et al. Rescue of amyotrophic lateral sclerosis phenotype in a mouse model by intravenous AAV9-ADAR2 delivery to motor neurons. *EMBO Mol Med* 2013;5: 1710–1719.
93. Lim JA, Yi H, Gao F, et al. Intravenous injection of an AAV-PHP.B vector encoding human acid alpha-glucosidase rescues both muscle and CNS defects in murine pompe disease. *Mol Ther Methods Clin Dev* 2019;12:233–245.
94. Papisov MI, Belov V, Fischman AJ, et al. Delivery of proteins to CNS as seen and measured by positron emission tomography. *Drug Deliv Transl Res* 2012;2:201–209.
95. Bailey SA, Zidell RH, Perry RW. Relationships between organ weight and body/brain weight in the rat: what is the best analytical endpoint? *Toxicol Pathol* 2004;32:448–466.
96. Ginn SL, Amaya AK, Alexander IE, et al. Gene therapy clinical trials worldwide to 2017: an update. *J Gene Med* 2018;20:e3015.
97. Wang D, Li S, Gessler DJ, et al. A rationally engineered capsid variant of AAV9 for systemic CNS-directed and peripheral tissue-detargeted gene delivery in neonates. *Mol Ther Methods Clin Dev* 2018;9:234–246.

Received for publication May 15, 2020;  
accepted after revision September 3, 2020.

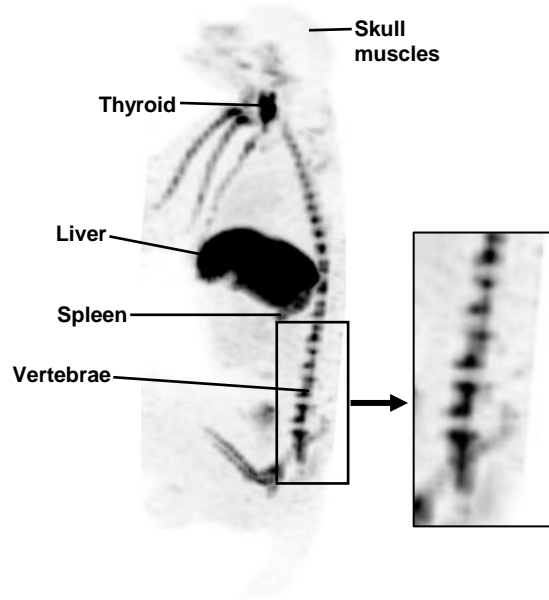
Published online: November 24, 2020.

**AAV capsid plus expression cassette****Organ-specific vector dosimetry**

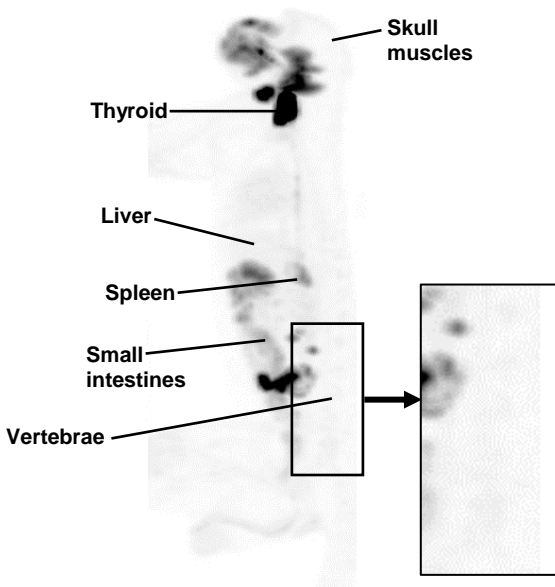
**A. AAVrh.10,  
intravenous, 24 hr**



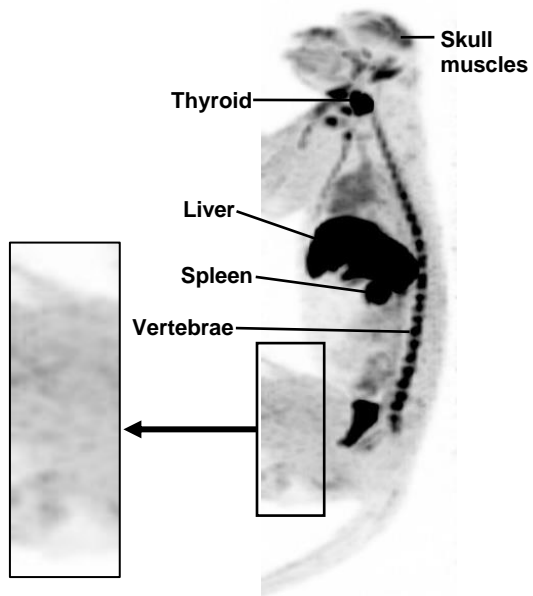
**B. AAV9,  
intravenous, 24 hr**



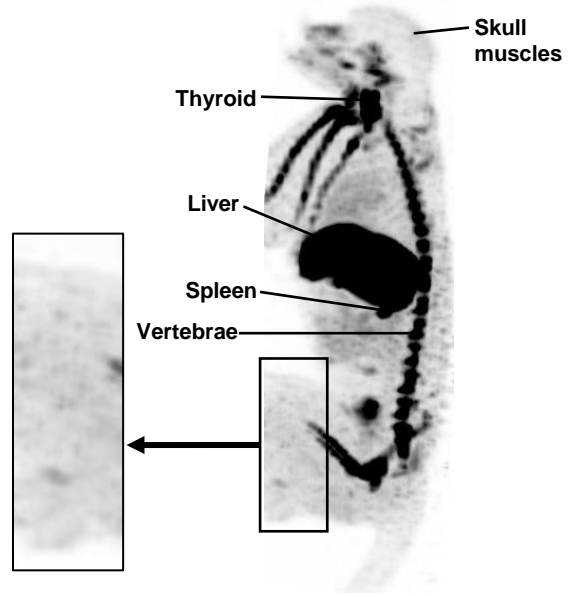
**C. Nal control,  
intravenous, 24 hr**



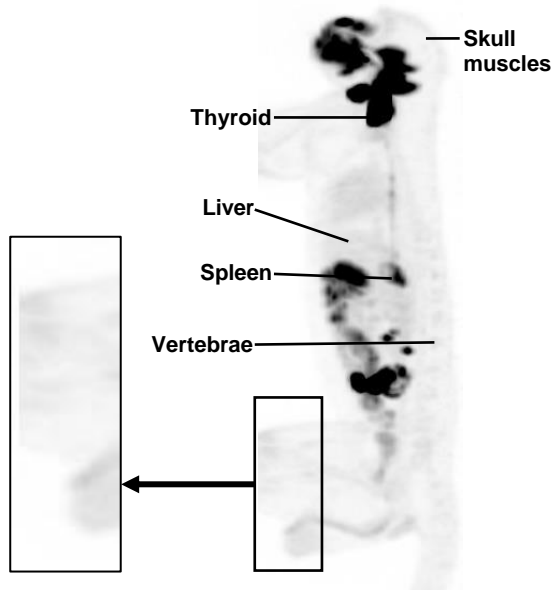
**A. Quadriceps AAVrh.10, intravenous**



**B. Quadriceps, AAV9, intravenous**



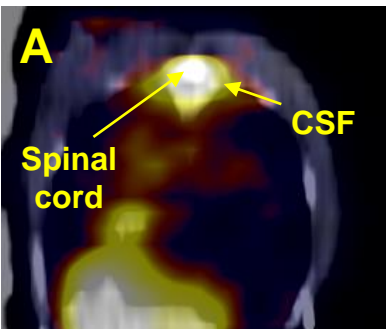
**C. Quadriceps, Nal intravenous**



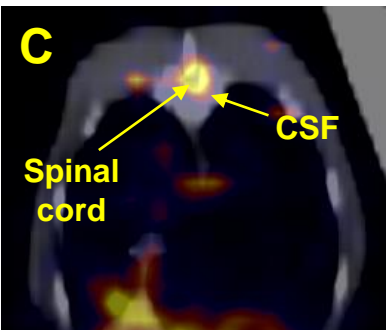
### Spine – axial section

### Spine – sagittal section

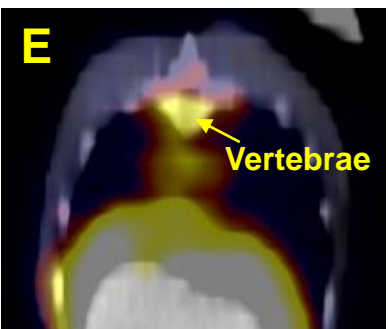
**AAV9mCherry,  
Intracisternal,  
24 hr**



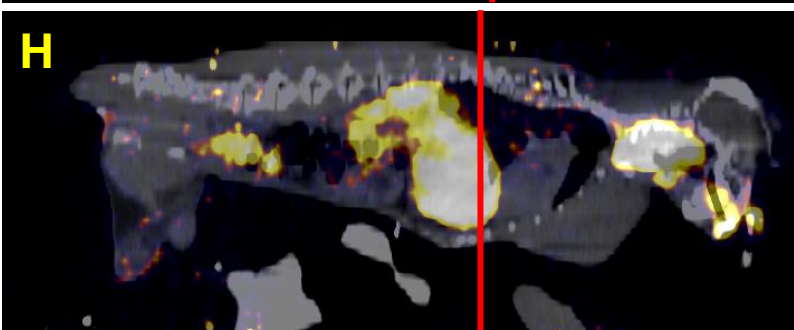
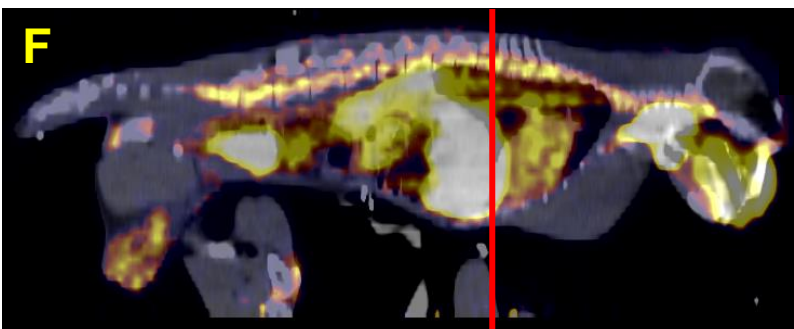
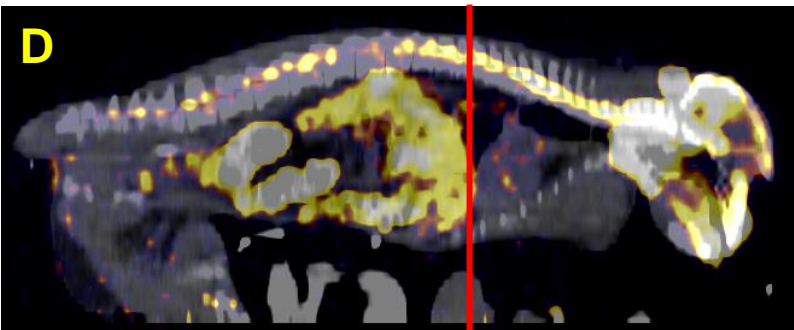
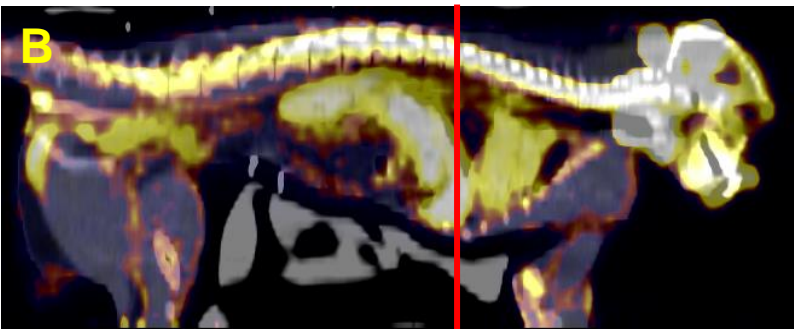
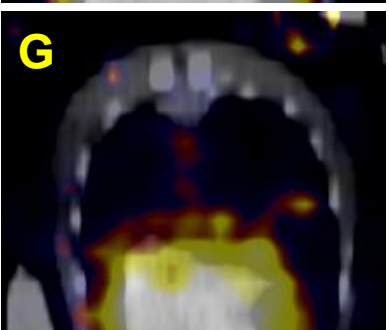
**AAV9mCherry,  
Intracisternal,  
72 hr**



**AAV9mCherry,  
Intravenous,  
24 hr**



**AAV9mCherry,  
Intravenous,  
72 hr**



**A. Nal control,  
intravenous, 24 hr**



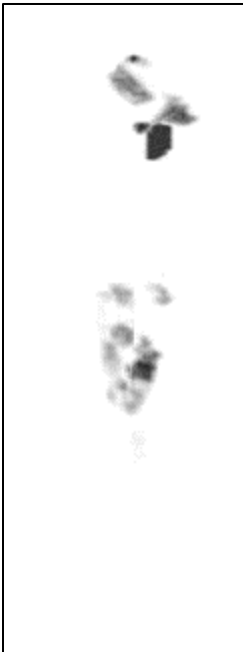
**B. AAVrh.10,  
intravenous, 24 hr**



**C. AAV9,  
intravenous, 24 hr**



**A. Nal control,  
intracisternal, 24 hr**



**B. AAVrh.10,  
intracisternal, 24 hr**



**C. AAV9,  
intracisternal, 24 hr**

